

AN EXTENSIVE CENSUS OF *HST* COUNTERPARTS TO *Chandra* X-RAY SOURCES IN THE GLOBULAR CLUSTER 47 TUCANAE. I. ASTROMETRY AND PHOTOMETRY<sup>1</sup>PETER D. EDMONDS<sup>2</sup>, RONALD L. GILLILAND<sup>3</sup>, CRAIG O. HEINKE<sup>2</sup>, & JONATHAN E. GRINDLAY<sup>2</sup>  
Draft version May 29, 2018

## ABSTRACT

We report, in this study of 47 Tucanae, the largest number of optical identifications of X-ray sources yet obtained in a single globular cluster. Using deep *Chandra*/ACIS-I imaging and extensive *HST* studies with WFPC2 (including a 120 orbit program giving superb *V* and *I* images), we have detected optical counterparts to at least 22 cataclysmic variables (CVs) and 29 chromospherically active binaries (BY Draconis and RS Canum Venaticorum systems) in 47 Tuc. These identifications are all based on tight astrometric matches between X-ray sources and objects with unusual (non main sequence) optical colors and/or optical variability. Several other CVs and active binaries have likely been found, but these have marginal significance because of larger offsets between the X-ray and optical positions, or colors and variability that are not statistically convincing. These less secure optical identifications are not subsequently discussed in detail.

In the *U* vs *U*−*V* color magnitude diagram (CMD), where the *U*-band corresponds to either F336W or F300W, the CVs all show evidence for blue colors compared to the main sequence, but most of them fall close to the main sequence in the *V* vs *V*−*I* CMD, showing that the secondary stars dominate the optical light. The X-ray detected active binaries have magnitude offsets above the main sequence (in both the *U* vs *U*−*V* or *V* vs *V*−*I* CMDs) that are indistinguishable from those of the much larger sample of optical variables (eclipsing and contact binaries and BY Dra variables) detected in the Wide Field Planetary Camera 2 (WFPC2) studies of Albrow et al. (2001). We also present the results of a new, deeper search for optical companions to MSPs. One possible optical companion to an MSP (47 Tuc T) was found, adding to the two optical companions already known. Finally, we study several blue stars with periodic variability from Albrow et al. (2001) that show little or no evidence for X-ray emission. The optical colors of these objects differ from those of 47 Tuc (and field) CVs.

An accompanying paper will present time series results for these optical identifications, and will discuss X-ray to optical flux ratios, spatial distributions and an overall interpretation of the results.

*Subject headings:* binaries: general – globular clusters: individual (47 Tucanae) – techniques: photometric – X-rays: binaries

## 1. INTRODUCTION

The study of globular cluster binaries is motivated by their profound impact on the dynamical evolution of globular clusters (Hut et al. 1992). Stellar densities near the centers of globular clusters can reach values as high as  $10^6$  stars per cubic parsec, and in these extreme conditions interactions and collisions between single and binary stars become inevitable (Hurley & Shara 2002). These interactions can act as a heating source by the conversion of binary binding energy into stellar kinetic energy when, for example, low-mass stars are ejected after binary collisions, helping to stall or prevent core collapse. Realistic models of globular cluster evolution therefore require knowledge of their binary star populations.

One of the most powerful ways to search for binaries in globular clusters is by studying their X-ray source population. The bright ( $L_x \gtrsim 10^{36}$  erg s<sup>−1</sup>) X-ray sources in globular clusters have already been identified with low-mass X-ray binaries (LMXBs; Grindlay et al. 1984) and the fainter sources ( $L_x \lesssim 10^{32-33}$  erg s<sup>−1</sup>) have long been thought to contain a mixture of LMXBs in quiescence (qLMXBs) and cataclysmic variables (CVs; Hertz & Grindlay 1983, Verbunt & Hasinger 1998). However, secure optical identifications were rare because of the severe crowding found near the centers of clusters. This problem is exacerbated by mass segregation, which causes relatively heavy objects like binaries to sink towards the centers of clus-

ters, where the crowding is at its worst. Because of these problems, only the brightest binaries in rich globular clusters like 47 Tucanae were discovered with X-ray missions like *Einstein* and ROSAT.

These resolution limitations have been dramatically overcome by the use of the *Chandra* X-ray observatory. Rich samples of X-ray sources have been reported in the globular clusters 47 Tuc (Grindlay et al. 2001a; hereafter GHE01a), NGC 6397 (Grindlay et al. 2001b; hereafter GHE01b), NGC 6752 (Pooley et al. 2002a), NGC 6440 (Pooley et al. 2002b) and  $\omega$  Centauri (Rutledge et al. 2002; Cool, Haggard, & Carlin 2002). The sample in the massive globular cluster 47 Tuc is by far the largest, with over 100 sources detected in a  $2' \times 2.5'$  field centered on the cluster (GHE01a), and close to 200 sources detected out to a radius of  $4'$  (Grindlay et al. 2002). These numbers for 47 Tuc alone outnumber the total sample of known X-ray sources in globular clusters before the availability of *Chandra*.

With the use of Hubble Space Telescope (*HST*) imaging, optical identifications of X-ray sources in several clusters have been reported (using both ROSAT and *Chandra* X-ray positions), including populations of CVs in NGC 6397 (Cool et al. 1998 and GHE01b) and NGC 6752 (Bailyn et al. 1996 and Pooley et al. 2002a). In 47 Tuc, Verbunt & Hasinger (1998) identified the ROSAT source X9 with the CV candidate V1 (Paresce,

<sup>1</sup> Based on observations with the NASA/ESA *Hubble Space Telescope* obtained at STScI, which is operated by AURA, Inc. under NASA contract NAS 5-26555.

<sup>2</sup> Harvard-Smithsonian Center for Astrophysics, 60 Garden St, Cambridge, MA 02138; pedmonds@cfa.harvard.edu; cheinke@cfa.harvard.edu, josh@cfa.harvard.edu

<sup>3</sup> Space Telescope Science Institute, 3700 San Martin Drive, Baltimore, MD 21218; gillil@stsci.edu

de Marchi, & Ferraro 1992) and X19 with the dwarf nova V2 (Paresce & de Marchi 1994). Other CV candidates in 47 Tuc include V3 (Shara et al. 1996) and AKO 9 (Auriere, Koch-Miramond, & Ortolani 1989 & Minniti et al. 1997).

The study by GHE01a used the  $0''.1$  internal<sup>4</sup> positional accuracy of *Chandra*, and deep *UVI* imaging of Gilliland et al. (2000; *HST* program GO-8267) to confirm the two optical identifications of Verbunt & Hasinger (1998) and found *Chandra* counterparts to V3 and AKO 9. A total of 13 optical identifications of CV candidates were found, the first detection of a substantial population of such objects in 47 Tuc. A large population of CVs in 47 Tuc was predicted by Di Stefano and Rappaport (1994), based on tidal capture and Monte Carlo simulations. A later archival *HST* study by Ferraro et al. (2001a) also reported identifications of V1, V2, V3 and AKO 9 with *Chandra* sources, and an *HST* study with the Space Telescope Imaging Spectrograph (STIS) by Knigge et al. (2002) reported UV counterparts for V1, V2, AKO 9 and W15 (a hard X-ray source identified by GHE01a as having a faint blue optical counterpart). These follow-up studies were limited by lack of sensitivity in the UV (Ferraro et al. 2001a) or by the small  $25'' \times 25''$  field of view (FoV) of the STIS camera (Knigge et al. 2002; only 21 of the 103 GHE01a sources are found in the STIS FoV).

Other classes of X-ray binary have been optically identified in 47 Tuc. GHE01a reported 6 optical identifications of chromospherically *active binaries*. In the galactic disk, active binaries include RS Canum Venaticorum (RS CVn) systems, typically consisting of a G- or K-type giant or subgiant with a late-type MS or subgiant companion, and BY Draconis (BY Dra) systems, typically consisting of two late-type MS stars (Dempsey et al. 1997). One of the active binaries identified by GHE01a shows a likely X-ray flare and is identified with an optical variable discovered by Edmonds et al. (1996). A handful of active binaries have also been observed in NGC 6397 (GHE01b) and NGC 6752 (Pooley et al. 2002a).

The sample of active binaries reported in this paper includes the X-ray detection of several red stragglers (also known as sub-subgiants), objects that are found just below the subgiant branch in globular and open clusters. Six of these objects were found in 47 Tuc by Albrow et al. (2001; hereafter AGB01), and others are known in NGC 6397 (GHE01b) and M67 (Mathieu et al. 2002). Some red stragglers are in exotic binary systems such as the subgiant secondary in the 47 Tuc CV AKO 9 and the optical companion to the MSP 6397-A in NGC 6397 (Ferraro et al. 2001b; Orosz & van Kerkwijk 2003). However, they do not always contain degenerate objects, since the recent study by Mathieu et al. (2002) of two red stragglers in M67 identified one of them (S1113) as likely having a  $1.3 M_{\odot}$  subgiant primary and a  $0.9 M_{\odot}$  MS secondary. However, despite detailed photometric (X-ray and optical), spectroscopic and proper-motion information, Mathieu et al. (2002) have been unable to provide a secure explanation for these objects.

Finally, three specialized papers have reported optical identifications of neutron star binaries in 47 Tuc: a qLMXB (Edmonds et al. 2002a) and two millisecond pulsars (MSPs) 47 Tuc U (Edmonds et al. 2001) and 47 Tuc W (Edmonds et al. 2002b). The 47 Tuc U binary companion is a He WD and the companion to 47 Tuc W is consistent with a heated main sequence star showing large amplitude orbital variations.

In this two-paper series, we report: (1) full details of the

CV and active binary optical identifications first reported by GHE01a, (2) a large number of new optical identifications using deeper photometric and time series analysis of the extensive GO-8267 dataset, plus a general search for optical companions to MSPs and qLMXBs and (3) analysis of archival F300W and V WFPC2 images obtained in *HST* program GO-7503 (PI: G. Meylan). The resulting set of optical IDs are by far the largest ever obtained for a globular cluster.

After a brief introduction to the data (§ 2), the astrometry for the optical counterparts will be described in § 3 and the optical photometry in § 4. The time series for these optical counterparts will be presented in Edmonds et al. (2003; hereafter Paper II). A detailed analysis section will also be given in Paper II, including a study of the spatial distribution of the sources and their X-ray to optical flux ratios.

## 2. OBSERVATIONS

### 2.1. X-ray data

The X-ray data used in this paper were obtained on 2000 March 16-17 and are described in detail in GHE01a. The detection limit of about 3 counts for these 72 ks, ACIS-I data corresponds to an X-ray luminosity, for an assumed 1 keV bremsstrahlung spectrum, and a 47 Tuc distance of 4.5 kpc (Heinke et al. 2003), of  $6 \times 10^{29} \text{ erg s}^{-1}$  (in the 0.5–2.5 keV band). This detection limit rises by factors of at least two or three within one core radius ( $r_c$ ) of the cluster center. For example only two (of 23) sources within  $0.5 r_c$  of the center have less than 12 counts.

We have retained the numbering used for the list of 108 sources given in GHE01a. This list was created by applying WAVDETECT to the standard level 2 event file, in energy band 0.5 to 4.5 keV, for a  $2' \times 2.5'$  central field. We have reprocessed the data using updated gain maps and removing the standard pipeline randomization of event location within each  $0''.5$  pixel<sup>5</sup>, slightly improving the resolution and astrometric quality of the *Chandra* data. We have used the new coordinates for each source in the original list, except for twelve sources that fell below our WAVDETECT threshold with the new processing because of crowding or low count levels; for these sources we use the original coordinates. Visual examination of the original and reprocessed images supports the reality of these 12 sources (as does the preliminary analysis of new, much deeper *Chandra* data). In the cases where sources are found in both the original and reprocessed lists, the positions typically differ by only  $0''.01$ – $0''.05$ .

We have also included sources detected in the reprocessed data within the  $2' \times 2.5'$  field, and beyond that field out to  $4'.0$  (extending beyond any of the *HST* data analyzed here). These sources are assigned names W109 to W193 (for concise reference to these sources in the text and figures we have avoided giving their *Chandra* convention source names). The subset of these new sources that are within either the GO-8267 or GO-7503 FoVs are listed in Table 1.

### 2.2. Optical data

The GO-8267 *HST* data (PI R. Gilliland) analyzed here is described in detail in Gilliland et al. (2000) and AGB01. This program involved an extensive set of 160 s WFPC2 exposures in F555W ('V'; 636 images) and F814W ('I'; 653 images) obtained over 8.3 days in 1999 July. The exposure times for the

<sup>4</sup> This refers to the astrometric accuracy within a *Chandra* image, while the accuracy of *Chandra*'s astrometric reference frame is  $0''.6$  (Aldcroft et al. 2000)

<sup>5</sup> See <http://asc.harvard.edu/ciao/threads/acispixrand/>

$V$  and  $I$  data were designed so that stars about half a magnitude brighter than the MS turn-off (MSTO) are saturated. In  $V$  this resulted in saturation for  $\sim 1.0\%$  of the pixels on the least crowded chip (WF3), and about 2% of pixels on the most crowded chip (WF2). In  $I$  the corresponding numbers are 1.5% and 2.8%. A limited number (28) of generally longer exposures in F336W ( $U'$ ) were also obtained, with negligible saturation levels (0.0002-0.001% of pixels). Sub-pixel dithering enabled deep, oversampled (by a factor of 4) images in  $U$ ,  $V$  and  $I$  to be produced. The magnitude limits reached for stars on the MS are  $U \sim 23.5$ ,  $V \sim 23.5$  (PC1 chip) to  $V \sim 25.0$  (WF3), and  $I \sim 21.5$  (PC) to  $I \sim 22.5$  (WF3). Crowding and enhanced background are the limiting factors in  $V$  and  $I$ .

The other optical dataset analyzed in detail is the program GO-7503 (PI G. Meylan) involving a short set of dithered F300W and  $V$  exposures with WFPC2 taken over six orbits about 110 days after GO-8267. The oversampled F300W image has comparable depth to the GO-8267  $U$  image. The GO-7503  $V$  image combines only 18 short (20 s) exposures and therefore has much lower signal-to-noise than the GO-8267  $V$  image, but the effective limiting depth (in the CMD) differs by  $\lesssim 1$  mag because of the effects of crowding in the GO-8267 data. Two earlier epochs of F300W data obtained as part of programs GO-5912 and GO-6467 are also briefly used in this paper in testing for long-term variability.

The FoVs of the GO-8267 and GO-7503 datasets are shown in Fig. 1 superimposed on the *Chandra* image. The GO-7503 program was obtained at a roll angle that differs significantly from the GO-8267 program, and hence the two FoVs are complementary. Also shown is the  $2' \times 2.5'$  field analyzed by GHE01a, the nominal center of the cluster (the average of the positions quoted by Guhathakurta et al. 1992, Calzetti et al. 1993 and de Marchi et al. 1996) and the  $24''$  core radius (Howell, Guhathakurta, & Gilliland 2000). A close-up of the center of the cluster is shown in Fig. 2. A total of 78 *Chandra* sources are found in the GO-8267 FoV and 84 in the GO-7503 FoV, with significant overlap between these two lists especially near the center of the cluster. A complete list of these sources and their chip locations is given in Table 2.

### 3. ASTROMETRY

We describe here the astrometric corrections used to shift the positions of the *Chandra* sources onto the *HST* coordinate frame (random errors for the WFPC2/*HST* coordinates determined by STSDAS/METRIC are assumed to be negligible). The optical identifications reported in GHE01a, Edmonds et al (2001), Edmonds et al. (2002a), Edmonds et al. (2002b), and those to be given here, were discovered using an iterative procedure, beginning with the X-ray identifications of the first three CV candidates to be discovered in 47 Tuc, V1 (Paresce, de Marchi, & Ferraro 1992), V2 (Paresce & de Marchi 1994) and V3 (Shara et al. 1996). The proposed astrometric matches of Verbunt and Hasinger (1998) between V1 and X9 (corresponding to *Chandra* source W42) and V2 and X19 (*Chandra* source W30) were adopted. Then, after applying the required offsets to the *Chandra* positions in Right Ascension (RA) and Declination (Dec), V3 was identified as a likely optical counterpart to X10 (W27). The rms values of the residuals after subtracting the 3 *HST* positions from the 3 corrected *Chandra* positions were determined to be  $0''.036$  in RA and  $0''.047$  in Dec. Since we show that V1, V2 and V3 are both blue (see § 4) and variable (see Paper II), and the chance of these matches being a coinci-

dence is extremely low (see § 4), these stars are confirmed as the optical counterparts of X9, X19 and X10 respectively.

Based on this determination of the *Chandra/HST* bore-site, we searched the GO-8267 data for optical variables and stars with colors outside those of the main sequence or giant branch. Any such objects lying within  $3\sigma$  of the positions of the *Chandra* sources, using the positional errors given by WAVDETECT, were identified as optical counterparts. Using the GO-8267 data we found 10 or more candidate optical counterparts for *Chandra* sources on each of the PC1, WF2 and WF4 chips. We then tested for linear correlations between the astrometric residuals and their positions, with appropriate weighting of each source using the errors estimated by WAVDETECT, and then removed this correlation. For both the PC1 and WF2 chips we found a significant correlation between the RA and RA residual, with constants of proportionality ( $a$ ) of  $0.0053 \pm 0.0011$  for the PC1 and  $0.0024 \pm 0.00049$  for WF2. For Dec no such correlations were found ( $a = 0.0009 \pm 0.0010$  for PC1, and  $a = 0.0003 \pm 0.0015$  for WF2). These results imply that systematic errors (of unknown origin) are present in the relative *HST-Chandra* positions, but even for stars near the extreme edges of the WF chips the astrometric corrections are small, no greater than  $\sim 0''.15$ . For the WF3 chip there were only 3 *Chandra* sources with optical counterparts, and here only the bore-site correction was calculated. For the WF4 chip we found a marginally significant correlation in RA, but with the opposite sign. Here, the astrometric solution is dominated by the only three sources (W21, W25 and W120) with more than 50 counts, and they are separated in RA by only  $\sim 18''$ , so the systematics are less accurately constrained. In Dec we found a marginal systematic error for WF4 ( $a = 0.0026 \pm 0.0011$ ).

For the 5 sources with more than 50 counts on the PC1 chip, the rms residuals in RA and Dec were determined to be  $0''.053$  and  $0''.035$  respectively before the linear corrections and  $0''.014$  and  $0''.035$  after the corrections. For WF2 the RA residual was reduced from  $0''.068$  to  $0''.050$  for the 5 sources with  $> 50$  counts (no significant change in Dec values) and for WF4 no significant improvement was found in RA but the Dec rms decreased from  $0''.075$  to  $0''.019$  for the 3 sources with  $> 50$  counts.

For comparison, we have performed a similar astrometric solution for the 6 most isolated X-ray counterparts to the MSPs. Here, we found the same apparent systematic error in the *Chandra* positions for RA, relative to the radio positions, with  $a = 0.0059 \pm 0.0021$ , a value consistent with that found for the *Chandra/HST* comparison (see also Edmonds et al. 2001). This confirms that there are small systematic errors in the *Chandra* positions. Deeper *Chandra* observations (recently obtained; see Paper II) will give much better source locations for the MSPs (and a more complete source list), and will allow further study of these subtle astrometric errors.

We included all of the optical IDs in a global astrometric solution, but here the brightest sources on the PC1 chip dominated the astrometry. Therefore, because different constants of proportionality were appropriate for each *HST* chip, and because we found small ( $\sim 0''.05 - 0''.1$ ) offsets between chips, this global solution gave larger errors than for the chip-by-chip solutions. Therefore, this procedure was discarded and the separate chip solutions were used.

Similar analysis was applied to the GO-7503 data and will not be described in detail here. Tables 3 and 4 show the RA and Dec offsets for all of our candidate optical counterparts

(W38, W92 and W94 positions were based on the randomized data used in GHE01a), including several marginal counterparts. Alternative designations for the optical IDs are given in Table 2. All of the counterparts are within  $3\text{-}\sigma$  of the quoted X-ray source (where the  $\sigma$  values are the WAVDETECT errors added to the systematic errors from our linear fits in quadrature), except for the marginal W71 counterpart at  $\sim 3.4\sigma$ , which we have included because the star is both blue and variable. Further discussion of the astrometry for this star will be given in Paper II. Finding charts for a sample of the optical counterparts are given in Fig. 3.

Besides the possible counterpart for W71, only the W43, W55, W75, W140 and W182 counterparts are at  $> 2.0\sigma$  (W73<sub>opt</sub> is at  $2.04\sigma$  in the GO-7503 data but is at  $1.89\sigma$  in GO-8267). Finding charts showing the *Chandra* image (0.5-8 keV) with these possible IDs overplotted are shown in Fig. 4 (W43, W55, W140 and W182) and Fig. 5 (the possible IDs for W71 and W75). The *Chandra* errors may have been underestimated for W43, W55 and W75 because they are close to cluster center and are relatively crowded. For example, the source W43 appears to be blended with a faint nearby source not detected with WAVDETECT, and W75 may be embedded in weak diffuse emission (possibly from a large number of weak sources). For W182 the presence of only 3 *Chandra* sources with likely optical counterparts on the WF3 chip has limited the accuracy of our astrometry. The likelihood of chance coincidences are described in § 4.

#### 4. PHOTOMETRY

The photometry analysis of the GO-8267 dataset used standard IRAF and DAOPHOT tools and customized software written by PDE. Since we required photometry for faint red stars (active binaries) as well as blue objects (CVs and MSPs), separate star lists were created for each filter and the DAOPHOT program ALLSTAR was run on each list. Stars were included in a color magnitude diagram (CMD) if they were detected in either all 3 filters or in *U* and *V* or *V* and *I* (the maximum matching distance between filters was 2 oversampled pixels). Objects with poor PSF fits and those with large amounts of light contamination from neighboring stars were removed. Despite this, a large number of artifacts remained in the *V* vs *V* - *I* CMD, caused by the effects of structure in the PSFs of bright (often saturated) stars in the very deep *V* and *I* images. More sophisticated techniques are required to improve the star lists and eliminate these artifacts, however these methods are unnecessary for this paper. Since the *U* image is affected less by artifacts (it is not as deep and the giant stars are not nearly as badly saturated), the *U* vs *U* - *V* CMD is much cleaner than the *V* vs *V* - *I* CMD. Since most of our X-ray counterparts are detected in *U*, and the exceptions are variables identified in *V* and *I* difference images, our list of X-ray IDs is likely to be clean of artifacts.

Calibration of the F336W, F555W and F814W magnitudes into *U*, *V* and *I* was performed using the zeropoints of AGB01 and the color corrections of Holtzman et al. (1995). The resulting *U* vs *U* - *V* and *V* vs *V* - *I* CMDs are shown in Figures 6 and 7, and close-ups of the region near the MSTO are shown in Fig. 8, where the data for all 4 chips is superimposed. Numerals are used to denote likely X-ray counterparts (using the numbering of GHE01a and our extended numbering system introduced earlier). Since several of the X-ray IDs are faint and crowded (CVs and a few active binaries) or are partly saturated (blue stragglers) we relaxed two of our CMD selection criteria

(crowding for the CV and active binary candidates and PSF-fit quality for the saturated blue stragglers) to plot the fullest possible set of X-ray IDs on this figure. There were several CV candidates where the PSF-fit quality in both the *V* and *I* bands exceeded our threshold and/or the position of the fitted star was more than 2 pixels away from the *U* band position (W15<sub>opt</sub>, W33<sub>opt</sub>, W45<sub>opt</sub>, W70<sub>opt</sub>). Here, *V* magnitude estimates were performed by iteratively using ADDSTAR to subtract PSF models of the star in the *V* image until the residuals were minimized. Larger errors were appropriate here than for the overall sample of stars, particularly for W33<sub>opt</sub> and W70<sub>opt</sub> where the *V* counterpart to the object detected in the *U* band is difficult to see in the oversampled images. However, in each case the stars are clearly blue by visual examination of the deep images (see Fig. 3). No such fitting was attempted in *I* where the crowding was even worse.

The analysis of the GO-7503 photometry (F300W and F555W) was carried out using the same PSF-fitting that was used for the GO-8267 analysis. The only difference in the analysis technique was that the deep oversampled images were created using the suite of drizzle routines (Hook, Pirzkal, & Fruchter 1999) available in STSDAS (these are designed to handle cosmic-ray removal with sparsely dithered data, unlike our customized software used for the GO-8267 analysis). The standard procedure recommended in the analysis guide was used, but with the two ‘SNR’ and one ‘scale’ parameters in `driz_cr` set to small values (1.0, 3.0; 2.5) to ensure as many cosmic rays were removed as possible. The disadvantage of this procedure is that some bright stars contained cores that were falsely identified as cosmic rays, but this did not affect our primary search for faint blue stars. The cosmic ray-cleaned F300W and F555W images for each epoch were combined into doubly oversampled images using the Drizzle routine. Because the GO-7503 data was mainly useful for detecting blue stars (CV or MSP candidates) that are brighter in the F300W image than in the F555W image, the deep F300W image was used to create a master star list. Using this star list, PSF-fitting was applied to both the F300W and F555W images using DAOPHOT programs. After applying a plate solution (using bright, relatively isolated stars used to build the PSF model) to transform the F555W coordinate frame to that of the F300W frame, stars  $< 2$  oversampled pixels apart in the two filters were considered detected in each. Extra filtering of the results was performed by eliminating stars with chi-squared values  $> 3$  and with ‘sharpness’ values  $> 1.2$  in the ALLSTAR output. Most of the stars with high chi-squared values were bright stars with central pixels that were mistaken for cosmic rays and were therefore truncated, distorting the PSF in the summed image. Since CVs are usually much fainter than the MSTO, the loss of a few bright MS stars and some giants did not affect our results. Stars with large sharpness values were generally PSF artifacts near bright stars. Figure 9 shows the CMDs resulting from this analysis, with labeling of likely or possible optical IDs to X-ray sources.

We also included stars detected in F300W but not in F555W. To avoid including large numbers of artifacts (mainly false stars detected in the PSF wings of bright stars) we set an upper limit on the total counts in a 2-pixel radius aperture in the F555W image. This limit did not seriously compromise our efforts to detect faint blue stars, since no candidate CVs were lost in this way. In cases where IDs are detected in F300W but not F555W the red limits are shown with arrows (the limits in F555W were determined from the  $3\sigma$  limit in the aperture counts). Other

such red limits are not shown in Fig. 9 to avoid confusion.

#### 4.1. Cataclysmic variables

Thirteen CV candidates in 47 Tuc have already been presented in GHE01a: V1 (W42), V2 (W30), V3 (W27), W1<sub>opt</sub>, W2<sub>opt</sub>, W8<sub>opt</sub>, W15<sub>opt</sub>, W21<sub>opt</sub>, W25<sub>opt</sub>, W36<sub>opt</sub> (AKO 9), W44<sub>opt</sub>, W45<sub>opt</sub> and W56<sub>opt</sub>. These are blue stars astrometrically matched ( $< 3\sigma$ ) to *Chandra* sources, and all but one of them are found in the GO-8267 FoV, and are plotted in Fig. 6. The exception (W56<sub>opt</sub>) was initially found in analysis of archival F300W data and is confirmed by the GO-7503 analysis (see below). Seven extra CV candidates (W33<sub>opt</sub>, W34<sub>opt</sub>, W35<sub>opt</sub>, W70<sub>opt</sub>, W120<sub>opt</sub> and W140<sub>opt</sub>, plus the marginal ID for W71) were found by closer examination of the GO-8267 images. Only two of these (W120<sub>opt</sub> and W140<sub>opt</sub>) were outside the  $2' \times 2.5'$  field analyzed by GHE01a.

The CV candidates in the GO-8267 data are all detected as clearly blue in the  $U$  vs  $U - V$  CMDs, with the exception of AKO 9 where the light in the  $U$  band has a significant contribution from the subgiant secondary. This star is redder in the  $V$  vs  $V - I$  CMD, where the subgiant dominates. A few of the CVs have blue  $V - I$  colors (e.g. W1<sub>opt</sub>, W21<sub>opt</sub> and V1), but most of them are found close to the MS ridge-line (although, as noted above, several of the optical counterparts were too faint or crowded to be detected by PSF-fitting in the  $I$  band). A similar result was found by Cool et al. (1998) for the CVs in NGC 6397 (we encourage detailed fitting to the broadband photometry of the CVs in both 47 Tuc and NGC 6397 to help constrain the properties of the accretion disk and compare with field CVs). A candidate ID for W35 is unfortunately affected by diffraction spikes in  $V$  and  $I$  (a saturated star with  $V=14.0$  is within  $0''.34$  or  $3.0\sigma$  of the nominal W35 position), but it does appear to be blue from visual examination.

In each of the GO-8267 CMDs the hydrogen WD models of Bergeron, Wesemael, & Beauchamp (1995) and the He WD models of Serenelli et al. (2001) are shown. Fig. 7 also shows CVs from the field surveys of Zwitter & Munari (1995), Zwitter & Munari (1996), and Munari & Zwitter (1998) and the 3 brightest He WDs and the 4 brightest CVs in NGC 6397 (Cool et al. 1998). Note the expected clear separation between the CVs (both field and cluster) and the cluster MS stars. Several of the 47 Tuc CVs have much redder  $V - I$  colors than the field and the NGC 6397 CVs.

Of the GO-8267 data CV candidates lying also in the GO-7503 FoV (V1, V2, V3, W15<sub>opt</sub>, W21<sub>opt</sub>, W25<sub>opt</sub>, W34<sub>opt</sub>, AKO 9, W44<sub>opt</sub>, W120<sub>opt</sub> and the marginal W71 ID) all are shown as blue stars in Fig. 9 except for V3 which fails both our chi-squared and sharpness tests (probably because large amplitude, short time-scale variability distorts the PSF in the process of combining the dithered images) and W120<sub>opt</sub> that lies just at the outer edge of the FoV. However, both of these exceptions are easily confirmed as blue stars by visual examination. A possible counterpart to W31 is in the FoV of both HST datasets but is only detected as a candidate blue star in the GO-7503 data. This is a marginal detection requiring confirmation with other data, since the possible blue object is close to a bright star, and is offset at the correct angle to be affected by diffraction spike artifacts. The possible CV identification for W35 also appears to be blue in the GO-7503 data, but the blue excess is clearly not as dramatic as for the CV candidates discussed above (Fig. 9), and we continue to classify this ID as marginal.

There are 8 blue stars and CV candidates that fall just in

the GO-7503 FoV (W49<sub>opt</sub>, W51<sub>opt</sub>, W53<sub>opt</sub>, W55<sub>opt</sub>, W56<sub>opt</sub>, W82<sub>opt</sub>, W85<sub>opt</sub> and W122<sub>opt</sub>). Only W56<sub>opt</sub> and W122<sub>opt</sub> were detected in both F300W and F555W. As noted above, the positional discrepancy is relatively large for W55<sub>opt</sub>.

From examination of Figures 6, 7 and 9 it is clear that there are significant numbers of blue objects found in the two datasets analyzed here. There are also blue stars that are detected in F300W but not F555W. To include both of these classes of object we identify stars as blue if they are (1) more than  $3\sigma$  bluewards of the MS or (2) if they are detected in F300W but not F555W and which have red limits that are also bluewards of the MS. Based on this analysis (for GO-7503), 181 blue stars were found on PC1, 256 on WF2, 170 on WF3 and 158 on WF4. These include a relatively small number of CVs (and possibly a few undetected MSPs) combined with cluster WDs and MS stars from the SMC, plus some artifacts. Given these large populations, we have calculated the probability that our astrometric matches between *Chandra* sources and blue stars are chance coincidences, based on the GO-7503 data (this has comparable depth to the GO-8267 data). We have calculated the number of blue stars (including stars with upper limits in F555W that appear to be blue) per unit area as a function of radial distance from the cluster center. We applied an evenly spaced grid (with individual grid elements of  $1''.6$ ) across the WFPC2 FoV and corrected for the incomplete radial coverage. To include the effects of crowding we deleted grid points with aperture counts in F555W greater than the threshold mentioned earlier. The resulting radial density function represents an upper limit to that of the true blue star population above our detection threshold because (a) PSF artifacts likely remain in our star list despite the quality controls applied to the PSF fitting results, and (b) elimination of grid points for counts above our threshold is only appropriate for stars detected only in F300W. Applying this function at the appropriate radial distance for each CV candidate and multiplying by  $\pi \times \text{offset}^2$  (where 'offset' is the *HST/Chandra* offset for each counterpart) to scale by area, we found probabilities of chance coincidences as given in the 6th column of tables 3 and 4. Note that only for W55, W71 and W140 are the probabilities  $> 4\%$ .

##### 4.1.1. Previous Observations

As noted in § 1 and § 3, and as shown in Table 2, several of the CVs presented here were discovered before GHE01a: V1 (Paresce, de Marchi, & Ferraro 1992), V2 (Paresce & de Marchi 1994), V3 (Shara et al. 1996) and AKO 9. The latter object is variable #11 from Edmonds et al. (1996), later identified with AKO 9 (Auriere, Koch-Miramond, & Ortolani 1989) by Minniti et al. (1997).

All 4 of the above objects have been identified in the *HST* survey of Ferraro et al. (2001a), with nominal angular separations between the *Chandra* sources and the blue stars of  $0''.0 - 0''.1$ . We believe that the majority of the other possible associations between *Chandra* sources and blue stars given in Table 5 of Ferraro et al. (2001a) are chance coincidences, and we note the appropriately tentative support given by Ferraro et al. (2001a) regarding the reality of these IDs. Except for the clearly identified objects described above, 17 of the 25 remaining suggested IDs have angular separations  $> 0''.9$ , and these typically have astrometric errors that are  $> 5\sigma$  (when using the *Chandra* derived errors) and in some cases are  $> 10\sigma$ . These offsets are much larger than those given in Tables 3 and 4, except for the few marginal candidates, and scaling from our numbers in Ta-

bles 3 and 4 the chances of coincidental matches with blue stars are considerable.

The objects with suggested IDs at large separations often include X-ray sources with more reasonable IDs presented here in Tables 3 and 4. For example, W15, W34 and W44 all have variable counterparts lying much closer to the X-ray position. The suggested blue straggler IDs for W31 and W37 have offsets of  $0''.4$  and  $0''.5$ , both worse than  $3\text{-}\sigma$  astrometrically (W31 has a marginal detection that lies considerably closer to the *Chandra* position). Also, W51 and W75 both have more likely IDs than those presented in Table 5 of Ferraro et al. (2001a; see below for further comments on the suggested match to W75). The possible ID for W98 appears to be only marginally blue in the  $m_{F218W}$  vs  $m_{F218W} - m_{F439W}$  CMD and lies at an unreasonably large angular separation of  $0''.7$ . We find no evidence of a blue star in our deep, oversampled images, although crowding from giants stars is a problem for this source. The remaining two suggested IDs are those for W54 and W80 at separations of  $0''.1$  and  $0''.2$ . We believe that the bright, red ID for W54 may be an RS CVn, but we see no evidence for a blue object (or a star with long-term variability) near W80.

The *HST*/STIS survey of Knigge et al. (2002) has identified the UV counterparts to V1, V2, AKO 9 and W15<sub>opt</sub>. None of the CV candidates of Knigge et al. (2002) are close to either W31 or W35, and no obvious star is nearby in the UV image apart from a bright blue straggler offset slightly from W31. This suggests that these two objects may not be CVs, although confirmation of this is needed by direct analysis of the UV image, since nearby bright stars may be preventing the detection of faint CVs in the *U*-band image (see also § 4.5). Several X-ray sources mentioned as having possible IDs from Ferraro et al. (2001a) fall in the Knigge et al. (2002) FoV. Of these, W31, W37 and W98 are not suggested by Knigge et al. (2002) as CV candidates. The possible ID for W75 (Knigge et al. 2002) will be discussed in Paper II. The general lack of detection of UV counterparts to X-ray sources by Knigge et al. (2002) will be discussed in § 4.3 and § 4.5.

#### 4.2. Blue Variables

In Figures 6 and 7 we also show blue variable stars that were discussed by AGB01 as possible CV candidates (PC1-V36, WF2-V08, WF2-V30, WF3-V06, WF3-V07, WF4-V05 and WF4-V26, abbreviated as 1V36, 2V08, 2V30, 3V06, 3V07, 4V05 and 4V26), but were not identified with X-ray sources by GHE01a. We have carefully examined these *blue variables* in the deep, oversampled *HST* images, and confirmed that all of them (except 4V26) have bluer colors than most other cluster stars, and are unaffected by artifacts (Table 5 lists the colors, positions and periods for these objects). Two blue, apparently variable objects from AGB01 were found to be possible artifacts: PC1-V52 has an irregular light curve but is not obviously blue and is found near a diffraction spike, and the apparent blue color and irregular variability of WF4-V16 appears to be caused by a bad pixel.

Most of the blue variables (4 out of 6; 3V06 does not have an *I* magnitude) are found in a region of the color-color plot where no field CVs are found, at  $0 \lesssim U - V \lesssim 0.4$ ,  $0 \lesssim V - I \lesssim 0.3$  (Fig. 10 shows a close-up of the color-color plot). Of the 5 objects in this area only W21<sub>opt</sub> is clearly an X-ray source, so it is the only strong CV candidate. The other two blue variables

(2V08 and 2V30) have significantly different colors, suggesting that they may represent a different class of object. Figure 5 shows the *Chandra* image (0.2–8 keV) with the blue variables (plus W21<sub>opt</sub>) overplotted as circles. Further discussion of these blue variables will be given in Paper II.

#### 4.3. Active Binaries

As shown by Tables 3 and 4 and Figures 6 and 7, a large number of the *Chandra* sources are astrometrically matched to optical variables with the colors of MS stars or subgiants (with no evidence for blue components). We believe the majority of these optical variables are active binaries (BY Drs or RS CVns), though a small fraction could be other possibilities such as MS stars with MSP companions (see Paper II). The clearest example of an active binary is the *Chandra* source W47 identified by GHE01a with optical variable #8 from Edmonds et al. (1996) and PC1-V08 from AGB01. The source W47 shows clear variability in the *Chandra* dataset (see Fig. 5 of GHE01a), a likely flare signature. Five other active binaries were reported by GHE01a: W14<sub>opt</sub>, W18<sub>opt</sub>, W41<sub>opt</sub>, W68<sub>opt</sub> and W43<sub>opt</sub>. The first three of these were also identified by AGB01 (and are also found in the GO-7503 field of view), the 4th is found in both the GO-8267 and GO-7503 datasets but fell just below the variability detection thresholds used in AGB01 (see below) and the 5th is a likely red straggler in the GO-7503 data (see Fig. 9). Red stragglers were defined by AGB01 as variable stars lying inside the following box in the CMD:  $0.8 < V - I < 1.5$ ;  $17.25 < V < 17.75$  (see Fig. 8), but obvious candidates are visible in CMDs using different broadband colors (see Fig. 9).

The 6 active binaries of GHE01a were selected using the conservative criterion for an active binary that the X-ray source be variable. This criterion is conservative because faint (5–20 ct) sources must show variability that is intrinsically extreme to be considered statistically significant. Two other active binary candidates are matched to variable X-ray sources (W92<sub>opt</sub> and W94<sub>opt</sub>), and an additional 20 optical variables and active binary candidates are matched to statistically non-variable X-ray sources.

Most of this large sample of active binary candidates have been independently discussed by AGB01 and include variables classified as eclipsing binaries (W12<sub>opt</sub>, W92<sub>opt</sub>, W137<sub>opt</sub>, & W182<sub>opt</sub>), W UMa binaries (W41<sub>opt</sub>, W47<sub>opt</sub>, & W163<sub>opt</sub>), a non-eclipsing contact and semi-detached binary (W66<sub>opt</sub>), red straggler variables (W3<sub>opt</sub> & W72<sub>opt</sub>) and ‘BY Dra’ variables<sup>6</sup> (W9<sub>opt</sub>, W14<sub>opt</sub>, W18<sub>opt</sub>, W69<sub>opt</sub>, W73<sub>opt</sub>, W75<sub>opt</sub>, & W76<sub>opt</sub>). Table 2 gives the AGB01 designations for each of these objects. Only the association between *Chandra* X-ray sources and some of the red stragglers was noted by AGB01.

A number of other optical variables in the GO-8267 FoV (not reported by AGB01) were discovered by searching carefully at the positions of X-ray sources. The new detections were for *Chandra* sources W22, W23, W26, W38, W59, W94, W121, W167, & W184. The ID for W59 was discovered with the single-pixel search method, where we searched for statistically significant periodicities in the time series of all individual pixels in the GO-8267 data-set (a valuable technique for detecting variable stars that are near artifacts such as saturation trails). This variable is near the edge of WF4 and is close to a bright neighbor. The ID for W167 (a blue straggler) was initially de-

<sup>6</sup> AGB01 use the term BY Dra for low amplitude variables on or close to the MS that do not appear to be eclipsing or contact systems, but we use this term in a more specialized sense to refer to systems that are both X-ray sources and optical variables containing two MS stars

tected as a variable but was then dropped from the AGB01 list because it is saturated. The other variables were not detected in the original AGB01 source list due to the faintness of the stars and crowding. The time series for these new variables will be discussed in Paper II.

Several other X-ray sources have possible identifications with stars that are either potential red stragglers or that have marginally significant variations in the optical (see Fig. 8). For continuity these results are quoted here, although most of the time series results are presented in Paper II. The possible ID for W4 is identified with a non-variable star near the blue side of the box in the CMD defining red stragglers, but without the detection of variability we classify this possible red straggler as a marginal candidate. The source W37 is a variable X-ray source within  $2\sigma$  of two bright ( $V=17.4$  and  $17.1$ ) MS stars. Either one of these stars could be an active binary but because variability is not observed we do not label them as such. The ID for W68, one of the original GHE01a active binaries, is a strongly variable ( $>99\%$  significance) X-ray source lying close to a star showing no obvious periodic variations in  $V$  but with a likely 1.12 day period in  $I$ . The false-alarm probability (FAP; Horne & Baliunas 1986) equals  $5.8 \times 10^{-4}$  at the power spectrum peak at 0.56 d. We consider this to be a reasonably secure detection. Finally, the marginal counterpart for W93 has a period of  $0.1122 \pm 0.002$  days and an amplitude of  $0.0016 \pm 0.0003$  ( $5.1\sigma$ ). If real, the orbital period is probably twice as long.

We now consider if any of these astrometric matches are likely to be chance coincidences. We calculated the spatial density of variables discovered by AGB01 for each of the 4 WFPC2 chips, scaling these densities by appropriate factors to account for variables not detected by AGB01 but subsequently found in deeper searches around the X-ray positions. Using this technique, we found that the largest chance probability for an active binary candidate is for W75<sub>opt</sub> (1.1%) and all of the other active binaries have chance probabilities  $<0.67\%$  (see the 6th column of Tables 3 and 4). Given these small probabilities we expect that the number of chance coincidences is negligible.

If the active binaries are double MS binaries then they should be found either on the MS or above it by  $\lesssim 0.75$  mag. We tested this hypothesis by measuring the distance of each of the active binaries above the MS ridge-line and comparing the distribution of these offsets with those found for the AGB01 binaries and the general stellar population. We performed iterative fits to the MS ridge-lines in both the  $U$  vs  $U-V$  and  $V$  vs  $V-I$  CMDs (after removing  $3-\sigma$  outliers) and then measured the vertical offsets ( $\Delta$  mag at fixed color) of each star from these fits. To avoid regions near the MSTO where the MS ridge-line is vertical (or close to it) we restricted our studies to regions with  $U > 18.4$  and  $V > 18$ , which imposed blue limits in  $U-V$  (0.53) and  $V-I$  (0.72). We only included X-ray IDs that survived the PSF quality and crowding tests presented in § 4 to ensure that the quality of the photometry is consistent with that of the general stellar population. The cumulative distributions of the vertical distance from the MS are shown in Fig. 11 for the 2 CMDs, where we plot the distributions for the active binaries, the AGB01 binaries and for all stars, excluding outliers with offsets greater than  $\pm 1.5$  mag (1.1% and 2.6% of the total stellar populations in the  $U$  vs  $U-V$  and  $V$  vs  $V-I$  CMDs).

In the  $U$  vs  $U-V$  CMD the set of active binaries includes the IDs for W12, W14, W18, W22, W41, W47, W69, W137, W182, & W184. The distribution of MS offsets for these objects is consistently brighter than the general stellar population,

as expected if they contain a significant number of binaries with reasonably bright secondaries (the median  $\delta mag$  offsets for the X-ray detected active binaries, the AGB01 binaries and the total stellar population are  $-0.27$ ,  $-0.07$  and  $0.001$  respectively). Using the KS-test there is a 99.21% probability that the distributions for the active binaries and the general stellar population are different (in this and in subsequent use of the KS-test we quote the probability that the distributions are different). This distribution is also somewhat brighter on average than that for the AGB01 binaries (KS probability = 62.6%), although the faint tail of the AGB01 distribution contains several likely spurious  $U$  values (from visual examination of the images) that skew the distribution to fainter values. In  $V$  vs  $V-I$  the active binary and AGB01 distributions are consistent with each other (KS probab. = 41.3 %) and they are both inconsistent with the general stellar distribution at  $> 99.999\%$  level (here the sample includes the binaries included in  $U$  vs  $U-V$  plus the IDs for W26, W59, W66, & W68). The ID for W23 is too near the vertical part of the MS to be included in this sample, and W94<sub>opt</sub> and W121<sub>opt</sub> are too crowded for reliable photometry (the light contamination from neighboring stars is too high; see § 4). Here, the median  $\delta mag$  offsets for the X-ray detected active binaries, the AGB01 binaries and the total stellar population are  $-0.42$ ,  $-0.47$  and  $0.014$  respectively.

The other active binaries are too bright to be included in this analysis. The IDs for W92, W163 and W167 are blue stragglers, while W9<sub>opt</sub> and W75<sub>opt</sub> (BY Dras) are found several tenths of a magnitude above the MSTO in both CMDs (see Fig. 8), consistent with them being binaries. The IDs for W3 and W72 have been classified as red stragglers (AGB01). The ID for W14 is found well to the red of the MS in both CMDs and is also a red straggler candidate (AGB01 found  $V=17.63$ ,  $U-V=0.87$ ,  $V-I=0.70$ ; we find  $V=17.61$ ,  $U-V=0.87$ ,  $V-I=0.89$ ). Note that W14<sub>opt</sub> also appears to be significantly redwards of the MS in the GO-7503 CMD (Fig. 9), consistent with the red straggler explanation. The IDs for W38 (an eclipsing binary) and W73 and W76 (both BY Dras) are all found close to the  $U$  vs  $U-V$  ridge-line but slightly to the red of the subgiant branch in  $V$  vs  $V-I$ , a possible hint to further red straggler type behavior (formally W38<sub>opt</sub> is found within the red straggler box shown in Fig. 8). Finally, in the  $V$  vs  $V-I$  CMD, W69<sub>opt</sub> is 1.56 mag brighter than the MS, but this object is not obviously a red straggler.

Active binaries generally should not have UV-bright components. This is consistent with the lack of detection (as CV candidates) of any of the 6 *Chandra* sources identified with active binaries (W14, W18, W26, W41, W73, W75) lying in the far-UV STIS image by Knigge et al. (2002). Knigge et al. (2002) suggest that the optical ID for W75 is 1V36 (V36 using their nomenclature), but an astrometric analysis shows that 1V36 is  $4.35-\sigma$  away from W75 and is therefore unlikely to be the ID for W75 (our proposed ID W75<sub>opt</sub> is  $2.3-\sigma$  away). However, the *Chandra* image (Fig. 5) does show enhanced counts near 1V36, possibly because it corresponds to a weak source. Deeper follow-up images with *Chandra* may confirm this possible detection. Further discussion of this interesting object will be given in Paper II.

We have not undertaken a general search of the GO-7503 dataset for variability (this dataset is clearly greatly inferior to the GO-8267 data for such searches) but a few likely and possible active binaries have been found in the GO-7503 data based on CMD position alone. By far the best candidate is W43<sub>opt</sub>(see

Fig. 9), a red straggler previously reported as a BY Dra by GHE01a. A possible counterpart to W64 is found above the MS and is a good active binary candidate, while W54 is a possible RS CVn, consistent with the Ferraro et al. (2001a) detection of a nearby bright object. Note that W64 is a bright source (164 counts) but shows no evidence for variability in the *Chandra* observation, unlike W47. However, it would probably have been detected in the ROSAT observations if it had been this bright, suggesting long-term variability.

#### 4.4. MSPs

Of the 20 MSPs reported by Camilo et al. (2000) and Freire et al. (2001), 13 are in binary systems and have companions that are potentially detectable in the optical, and all but 47 Tuc J fall in at least one of the GO-8267 or GO-7503 FoVs. The secondary star masses are predicted by Camilo et al. (2000) to either fall in a relatively high mass range of  $\sim 0.15\text{--}0.2M_{\odot}$  (47 Tuc E, H, Q, T, S, U, W) or  $0.02\text{--}0.03M_{\odot}$  (47 Tuc I, J, O, P, R). The MSP 47 Tuc V is believed to have a relatively massive companion, but more detections of this object are required to give a mass estimate.

A previous search (using the GO-8267 data) was made for blue optical counterparts to binary MSPs (Edmonds et al. 2001) in the cases where the MSPs were detected as X-ray sources using WAVDETECT (see GHE01a and Grindlay et al. 2002) and the radio sources have timing positions (47 Tuc E, H, I, O, and U). One obvious optical counterpart to an MSP in this cluster (47 Tuc U), with an associated *Chandra* source (W11) was discovered by Edmonds et al. (2001). This blue star is almost certainly a He WD and shows small amplitude orbital variations at the same period and phase as the radio binary. We have found no other unambiguous association of blue stars and MSPs in searching the optical images at the positions of the radio/X-ray MSPs.

For 47 Tuc E (*Chandra* source W7), several stars, some of them relatively bright, are found within the  $3\sigma$  error circle. The power spectra of two nearby ( $< 3\sigma$ ) MS stars with  $V=17.9$  &  $18.5$  show no evidence for periodic or non-periodic variability. Difference images<sup>7</sup> were calculated for these stars and then the period and phase of the radio MSP was used to create mean difference images within  $\pm 0.07$  in orbital phase of the expected maximum and minimum light. These showed no evidence for a periodic signal (ie a stellar shaped source). The MSP 47 Tuc H (W74) is found in a relatively blank region of 47 Tuc and we are able to set upper limits in  $U$  and  $V$  of 25.8 and 23.7 respectively. No stars with non-MS colors or variability were found within the error circle of the MSP 47 Tuc O (W39).

To look for binary MSP counterparts in the cases where no X-ray source was detected with WAVDETECT (47 Tuc Q and T), we used the astrometry techniques given in § 3 (and used in Grindlay et al. 2002) to shift the radio coordinate frame onto the X-ray coordinate frame using the 6 relatively isolated MSPs detected with *Chandra*. The resulting positional errors for the 16 MSPs after making these linear fits were dominated by the relatively large errors ( $0''.1\text{--}0''.15$ ) in the X-ray positions (the radio errors are a few milliarcseconds). Then the corrected X-ray positions were transformed to the *HST* coordinate frame, on a chip-by-chip basis, using the large number of optical counterparts to X-ray sources, with the smaller errors for this transformation (compared to the radio to X-ray transformation) propagated into the final MSP errors.

Using this astrometry, one likely, very faint ( $U \sim 23.8$ ; see Fig. 6) blue star is found on the WF2 chip only  $0.11''$  ( $0.9\sigma$ ) from the position of 47 Tuc T (Fig. 12 shows a finding chart). No corresponding star is visible in the  $V$  or  $I$  images in the PSF wings of a neighboring red star, showing that the possible MSP counterpart is indeed blue (faint MS stars will appear to be much fainter in the  $U$  image than in the  $V$  or  $I$  image). If this star is a He WD then using the He WD cooling curves of Serenelli et al. (2001) corrected to the 47 Tuc distance and reddening (see Fig. 6) we infer that the star has a cooling age  $\lesssim 0.5$  Gyr if the WD mass is  $\gtrsim 0.2 M_{\odot}$ , and a cooling age of  $\sim 10$  Gyr if the WD mass is  $\sim 0.17M_{\odot}$  (the lowest mass model of Serenelli et al 2001). Since perhaps only future generation telescopes are likely to produce deeper  $V$  images of 47 Tuc than this dataset, it may be some time before useful constraints on the WD cooling age are made from optical color information. A possible blue star also exists within  $0.09''$  ( $0.82\sigma$ ) of 47 Tuc I (W19), however in this case the possible  $U$ -bright star is much more crowded than the candidate near 47 Tuc T, and is only a marginal candidate at best. The PSF is not unambiguously stellar and could, e.g. be the combination of light from several unresolved stars. The derived  $U$  magnitude is  $\sim 24$  and the extreme crowding is likely to limit useful follow-up observations at optical wavelengths, but UV observations with ACS/HRC may provide useful constraints. The detection of an optical counterpart to 47 Tuc I would be of great interest, since this MSP has a very low mass companion (no optical companions for such objects have been detected in globular clusters).

For 47 Tuc Q there is one bright ( $V = 17.7$ ) star only  $0''.24$  ( $1.3\sigma$ ) away from the corrected MSP position, and this star is found on the MS near the turnoff ('nQ' in Fig. 6). This shows no evidence for a power spectrum signal at the 1.189 day binary period detected in the radio, but it does show evidence for a signal in the  $V$ -band with period =  $(0.391359 \pm 0.001700)$  days and amplitude =  $0.00144 \pm 0.00017$  ( $8.5\sigma$ ). This period is  $\sim 3\sigma$  away from being one third of the period of 47 Tuc Q. No interesting signal is seen in  $I$ . Since the binary orbit of 47 Tuc Q is very close to circular (Freire et al. 2001), this shorter period is unlikely to represent evidence for enforced, rapid rotation at periastron in a highly elliptical orbit. Therefore, we believe this possible optical counterpart is most likely a chance coincidence.

The binary MSP 47 Tuc S (W77), thought to have a He WD companion (Camilo et al. 2000), falls in the GO-7503 FoV but no blue stars are visible by comparing the F300W and F555W images. Four of the MSPs (47 Tuc P, R, V and W) from the sample of Freire et al. (2001) do not have timing positions, and one of these (47 Tuc W) has been identified with the optically variable star W29<sub>opt</sub> by Edmonds et al. (2002b). The prospects of further discoveries like this are discussed in Paper II.

#### 4.5. Unidentified X-ray sources

There are only a small number (8) of moderately bright ( $> 20$  ct) *Chandra* sources in the GO-8267 source list without plausible optical counterparts. The source W46 is almost certainly a qLMXB based on the X-ray luminosity and spectrum (GHE01a and Heinke et al. 2003) but has no plausible optical counterpart (Edmonds et al. 2002a). The possible CV ID for W35 was discussed in § 4.1. The source W16 (102 cts) falls in a very crowded part of the *HST* image (it lies  $0.6''$  from a bright, variable red giant). Its nearest counterparts in the  $U$  images are at

<sup>7</sup> Difference images are generated by subtracting from each individual image the mean over-sampled image evaluated at the appropriate dither position; see AGB01

1.2, 3.8 and 3.9  $\sigma$  with  $U$  mags of 21.4, 18.3 and 20.5 respectively, but the effects of the giant star severely limit results in  $V$  and  $I$ . Because of the hard X-ray spectrum and its reasonably high luminosity this source is most likely a CV. Finally, W17 is discussed in Paper II as a possible CV or qLMXB.

The sources W20, W24, W32 and W37 all have bright, but apparently non-variable stars within  $3\sigma$  of the X-ray positions (W20 has a  $V=17.6$  star at  $0.44\sigma$ ; W24 a  $V=16.0$  star at  $1.35\sigma$ ; W32 a  $V=17.5$  star at  $1.48\sigma$ ; W37 was discussed in § 4.3). Presumably these bright stars could be active binaries with low inclinations giving a small observed amplitude for orbital variations (and the star near W24 is saturated, so the time series have lower quality than available for MSTO stars), or they could be overpowering the light of fainter optical IDs, such as CVs. Also, the bright star near W24 is found on the blue side of the giant branch (based on preliminary photometry of short exposures), suggesting binarity. Although none of these objects are suggested as CV candidates by Knigge et al. (2002), their CMD uses a color based on far-UV and F336W magnitudes, and the light contamination from the nearby MS stars and subgiants may prevent the detection of fainter objects in F336W that represent the true counterparts. However, MSTO stars and subgiants are much fainter in the far-UV and therefore, close examination of the images of Knigge et al. (2002), and spectroscopic and variability studies of nearby UV stars should be useful in searching for CV counterparts in the UV. These 4 *Chandra* sources may also have MSP counterparts, but they are all brighter than the most luminous MSP and the faintest (W37) is a variable X-ray source.

Several of the fainter ( $< 20$  ct), unidentified sources, have saturated stars nearby that may have prevented the detection of faint objects like CVs. The source W10 has a saturated star ( $V=15.3$ ) within  $0''.27$  ( $2.4\sigma$ ), W31 has a saturated star ( $V=15.9$ ) within  $0''.23$  ( $2.1\sigma$ ), W98 has 3 saturated stars ( $V=15.1-16.0$ ) within  $0''.4$  ( $2.0\sigma$ ), W115 has a saturated star ( $V=17.0$ ) within  $0''.3$  ( $2.1\sigma$ ), W141 has a saturated star ( $V=14.0$ ) within  $0''.22$  ( $1.5\sigma$ ), and W168 has a saturated star ( $V=13.6$ ) within  $0''.16$  ( $0.7\sigma$ ). Several of these examples (especially W168 and W141) may represent the detection of the saturated star itself, most likely as an RS CVn.

## 5. DISCUSSION

### 5.1. Cataclysmic variables

We have discovered (or confirmed) optical counterparts for 22 *Chandra* sources that are likely CVs as summarized in Tables 3 and 4 (we have included V3 in this list, but it may be a qLMXB, as discussed in Paper II). Edmonds et al. (2002b) tentatively classified W34<sub>opt</sub> as an MSP companion based on the similarity of its  $V$  and  $I$  light curves with the 47 Tuc W companion, but it may also be a CV. Alternatively, a small number of MSPs may be included in our CV sample, as discussed in Paper II. Among the marginal candidates given in Tables 3 and 4 we believe that W140<sub>opt</sub> and W55<sub>opt</sub> (see Fig. 4) have the greatest chances of being CVs, although the chance of astrometric coincidences is now significant (4.1% and 10.8%).

This is easily the largest sample of CVs detected in a single globular cluster. The photometric properties of these stars are summarized as: (1) they all have  $U-V$  or F300W-F555W colors that place them well bluewards of the MS, with the exception of AKO 9 (with its bright secondary); (2) the optical IDs for W2, W8, W25, V2, V3, W44 and W120 all lie on or close to the MS in  $V$  vs  $V-I$  (similar behavior is seen in the CVs discov-

ered in NGC 6397 and NGC 6752), while only V1, W1<sub>opt</sub> and W21<sub>opt</sub> and possibly W34<sub>opt</sub> are found well to the blue of the MS. These results show that the secondaries generally dominate the optical light and that the accretion disks are relatively faint, suggesting that these systems have low accretion rates. Strong support for this hypothesis is given in Paper II, where the periods for some of these objects, and their absolute magnitude, X-ray luminosity and  $F_X/F_{opt}$  distributions will be presented.

Unfortunately, because of crowding in the *HST* images, our sample of CVs does not reach the very faint absolute magnitudes ( $M_V > 10$ ) discussed by Townsley & Bildsten (2002) in their modeling of low accretion rate CVs with periods below the period gap. For making direct comparison with the  $V$  and  $I$  magnitudes predicted by Townsley & Bildsten (2002), matters are even worse because: (1) some of the faintest CVs in the GO-8267 FoV lack  $I$  magnitudes (e.g. W15<sub>opt</sub> & W70<sub>opt</sub>), and (2) the CVs found only in the GO-7503 FoV all lack  $I$  magnitudes (and, in many cases, F555W magnitudes). A couple of the faintest CV candidates (W34<sub>opt</sub> & W140<sub>opt</sub>) do have bluer colors than the MS, suggesting a greater contribution from the WD, as predicted by Townsley & Bildsten (2002) at faint magnitudes. However, W34<sub>opt</sub> could be an MSP, and W140<sub>opt</sub> is only a marginal CV candidate, and even if they are CVs, their bluer colors could be explained by either relatively bright accretion disks or lower inclinations than average.

We do not find convincing evidence for X-ray emission from the blue variables discussed by AGB01, although one of these objects (1V36) may be a weak, crowded X-ray source; see also the discussions of the UV and optical properties of 1V36 in Ferraro et al. (2001a) and Knigge et al. (2002). Possible explanations for these blue variables will be discussed in Paper II.

### 5.2. Active binaries

Adding up the total number of active binary candidates in Tables 3 and 4 (counting only W43 and W64 of the GO-7503 data candidates) we have observed a total of 29 likely active binaries. Except for W43<sub>opt</sub> and W64<sub>opt</sub>, all of these are found in the GO-8267 FoV and show statistically significant, mostly periodic, variability (see Paper II). They are mostly found on, or slightly above, the MS or subgiant ridge-line except for W69<sub>opt</sub> and a handful of red stragglers or red straggler candidates. Several marginal active binaries have also been found. The total sample of active binaries in 47 Tuc above our X-ray detection threshold will inevitably be larger, and in particular a number of MS-MS binaries that were outside the GO-8267 FoV should be found in the GO-7503 FoV.

### 5.3. Summary

Almost certain matches are available for 45 of 78 X-ray sources within the extensive *HST*/WFPC2 imaging of program GO-8267 on the basis of tight astrometric pairing with optical sources showing unusual CMD locations and/or clear optical variability. Six of the remaining sources in the GO-8267 field are solitary MSPs or binary MSPs (with likely He WD companions) from Camilo et al. (2000), and one of the remaining sources is a qLMXB (GHE01a; Edmonds et al. 2002a; Heinke et al. 2003), and each of these neutron star systems are expected to have faint or extremely faint optical counterparts. Of the remaining 26 sources,  $\sim 15$  are problematic due to astrometric coincidence with regions of low data quality (e.g. covered by saturation trails or extremely crowded; see Paper II for

more details), and  $\lesssim 4$  lack optical IDs in clean regions of optical coverage (here the working explanation is that these sources are MSPs and the optical counterparts fall below the detection limit of even the extensive *HST*/WFPC2 observations available to us). Of the 84 X-ray sources found within the GO-7503 FoV, 52 are also found in the GO-8267 FoV, and of the remaining 32 sources, 10 have optical identifications.

Paper II will present the time series results for these optical identifications, plus a detailed analysis section, including

a study of the spatial distribution of the optical identifications, and the distributions of their absolute magnitudes, X-ray luminosities and X-ray to optical flux ratios. This will be followed by an overall interpretation of the results.

This work was supported in part by STScI grants GO-8267.01-97A (PDE and RLG) and HST-AR-09199.01-A (PDE). We acknowledge several helpful comments from the referee, Christian Knigge.

## REFERENCES

- Albrow, M. D., Gilliland, R. L., Brown, T. M., Edmonds, P. D., Guhathakurta, P., & Sarajedini, A. 2001, *ApJ*, 559, 1060 (AGB01)
- Aldcroft, T. L., Karovska, M., Cresitello-Dittmar, M. L., Cameron, R. A., & Markevitch, M. L. 2000, *Proc. SPIE*, 4012, 650
- Auriere, M., Koch-Miramond, L., & Ortolani, S. 1989, *A&A*, 214, 113
- Bailyn, C. D., Rubenstein, E. P., Slavin, S. D., Cohn, H., Lugger, P., Cool, A. M., & Grindlay, J. E. 1996, *ApJ*, 473, L31
- Bergeron, P., Wesemael, F., & Beauchamp, A. 1995, *PASP*, 107, 1047
- Calzetti, D., de Marchi, G., Paresce, F., & Shara, M. 1993, *ApJ*, 402, L1
- Camilo, F., Lorimer, D. R., Freire, P., Lyne, A. G., & Manchester, R. N. 2000, *ApJ*, 535, 975
- Cool, A. M., Grindlay, J. E., Cohn, H. N., Lugger, P. M., & Bailyn, C. D. 1998, *ApJ*, 508, L75
- Cool, A. M., Haggard, D., & Carlin, J. L. 2002, *ASP Conf. Ser.* 265: Omega Centauri, A Unique Window into Astrophysics, 277
- de Marchi, G., Paresce, F., Stratta, M. G., Gilliland, R. L., & Bohlin, R. C. 1996, *ApJ*, 468, L51
- Dempsey, R. C., Linsky, J. L., Fleming, T. A., & Schmitt, J. H. M. M. 1997, *ApJ*, 478, 358
- Di Stefano, R. & Rappaport, S. 1994, *ApJ*, 423, 274
- Edmonds, P. D., Gilliland, R. L., Guhathakurta, P., Petro, L. D., Saha, A., & Shara, M. M. 1996, *ApJ*, 468, 241
- Edmonds, P. D., Grindlay, J. E., Cool, A., Cohn, H., Lugger, P., & Bailyn, C. 1999, *ApJ*, 516, 250
- Edmonds, P. D., Gilliland, R. L., Heinke, C. O., Grindlay, J. E., & Camilo, F. 2001, *ApJ*, 557, L57
- Edmonds, P. D., Heinke, C. O., Grindlay, J. E., & Gilliland, R. L. 2002a, *ApJ*, 564, L17
- Edmonds, P. D., Gilliland, R. L., Camilo, F., Heinke, C. O., & Grindlay, J. E. 2002b, *ApJ*, 579, 741
- Edmonds, P. D., Gilliland, R. L., Heinke, C. O., & Grindlay, J. E. 2003, *ApJ*, submitted (Paper II)
- Ferraro, F. R., D'Amico, N., Possenti, A., Mignani, R. P., & Paltrinieri, B. 2001a, *ApJ*, 561, 337
- Ferraro, F. R., Possenti, A., D'Amico, N., & Sabbi, E. 2001b, *ApJ*, 561, L93
- Freire, P. C., Camilo, F., Lorimer, D. R., Lyne, A. G., Manchester, R. N., & D'Amico, N. 2001, *MNRAS*, 326, 901
- Gilliland, R. L. et al. 2000, *ApJ*, 545, L47
- Grindlay, J. E., Hertz, P., Steiner, J. E., Murray, S. S., & Lightman, A. P. 1984, *ApJ*, 282, L13
- Grindlay, J. E., Heinke, C. O., Edmonds, P. D. & Murray, S. 2001a, *Science*, 292, 2290 (GHE01a)
- Grindlay, J. E., Heinke, C. O., Edmonds, P. D., Murray, S. S., & Cool, A. M. 2001b, *ApJ*, 563, L53 (GHE01b)
- Grindlay, J. E., Camilo, F., Heinke, C. O., Edmonds, P. D., Cohn, H., & Lugger, P. 2002, *ApJ*, 581, 470
- Guhathakurta, P., Yanny, B., Schneider, D. P., & Bahcall, J. N. 1992, *AJ*, 104, 1790
- Heinke, C. O., Grindlay, J. E., Lloyd, D. & Edmonds, P. D. 2003, *ApJ*, accepted
- Hertz, P. & Grindlay, J. E. 1983, *ApJ*, 275, 105
- Hook, R. N., Pirzkal, N., & Fruchter, A. S. 1999, *ASP Conf. Ser.* 172: Astronomical Data Analysis Software and Systems VIII, 8, 337
- Holtzman, J. A., Burrows, C. J., Casertano, S., Hester, J. J., Trauger, J. T., Watson, A. M., & Worthey, G. 1995, *PASP*, 107, 1065
- Horne, J. H. & Baliunas, S. L. 1986, *ApJ*, 302, 757
- Howell, J. H., Guhathakurta, P., & Gilliland, R. L. 2000, *PASP*, 112, 1200
- Hurley, J. R. & Shara, M. M. 2002, *ApJ*, 570, 184
- Hut, P. et al. 1992, *PASP*, 104, 981
- Knigge, C., Zurek, D. R., Shara, M. M., & Long, K. S. 2002, *ApJ*, 579, 752
- Mathieu, R. D., van den Berg, M., Torres, G., Latham, D., Verbunt, F., & Stassun, K. 2002, *astro-ph/0209568*
- Minniti, D., Meylan, G., Pryor, C., Phinney, E. S., Sams, B., & Tinney, C. G. 1997, *ApJ*, 474, L27
- Munari, U. & Zwitter, T. 1998, *A&AS*, 128, 277
- Orosz, J. A. & van Kerkwijk, M. H. 2003, *A&A*, 397, 237
- Paresce, F., de Marchi, G., & Ferraro, F. R. 1992, *Nature*, 360, 46
- Paresce, F. & de Marchi, G. 1994, *ApJ*, 427, L33
- Pooley, D. et al. 2002a, *ApJ*, 569, 405
- Pooley, D. et al. 2002b, *ApJ*, 573, 184
- Rutledge, R. E., Bildsten, L., Brown, E. F., Pavlov, G. G., & Zavlin, V. E. 2002, *ApJ*, 578, 405
- Serenelli, A. M., Althaus, L. G., Rohrmann R. D. & Benvenuto, O. G. 2001, *MNRAS*, 325, 607
- Shara, M. M., Bergeron, L. E., Gilliland, R. L., Saha, A., & Petro, L. 1996, *ApJ*, 471, 804
- Sills, A., Bailyn, C. D., Edmonds, P. D., & Gilliland, R. L. 2000, *ApJ*, 535, 298
- Townsley, D. M. & Bildsten, L. 2002, *ApJ*, 565, L35
- Verbunt, F. & Hasinger, G. 1998, *A&A*, 336, 895
- Zoccali, M. et al. 2001, *ApJ*, 553, 733
- Zwitter, T. & Munari, U. 1995, *A&AS*, 114, 575
- Zwitter, T. & Munari, U. 1996, *A&AS*, 117, 449

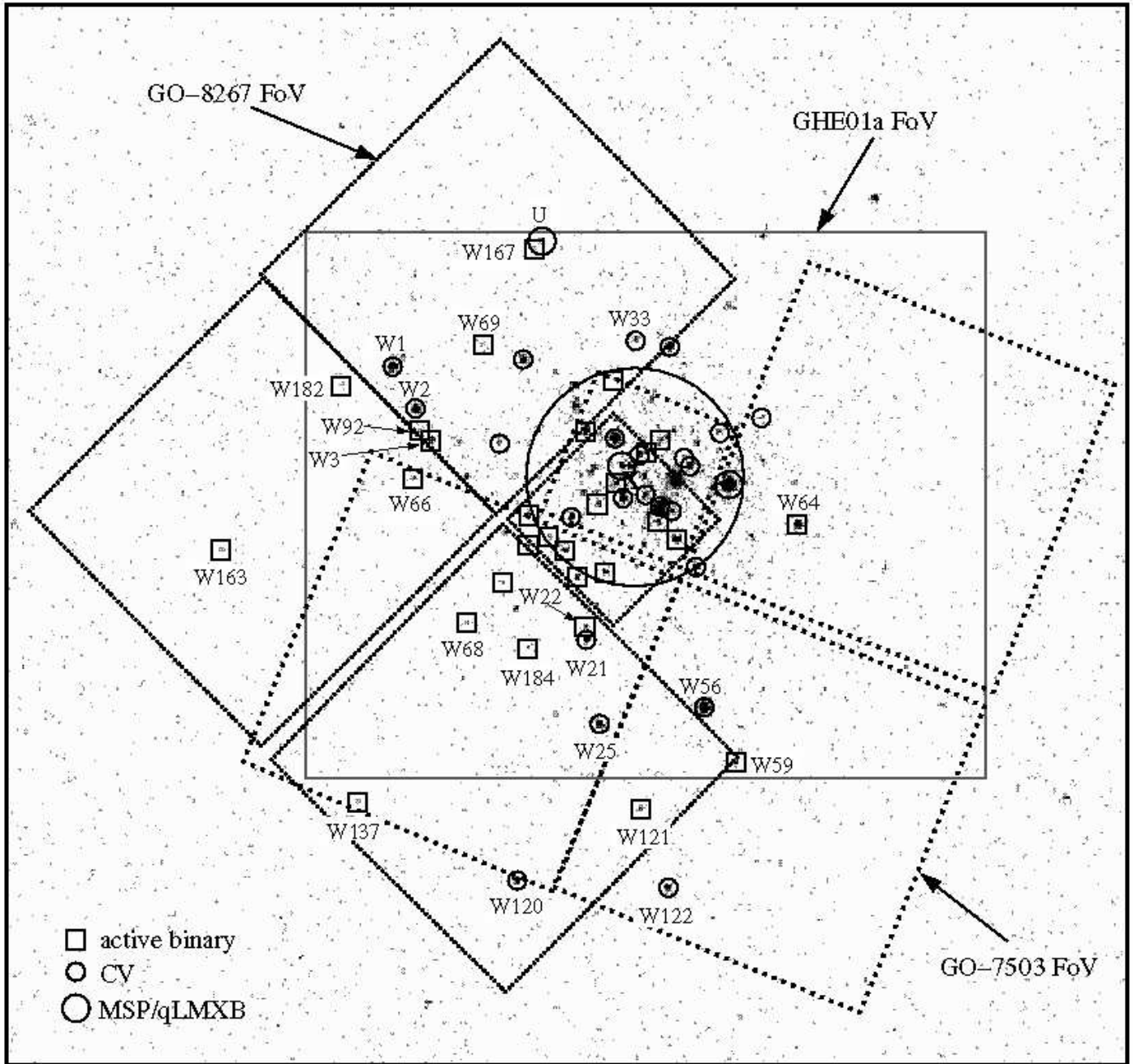


FIG. 1.— A *Chandra* image of 47 Tuc with the WFPC2 FoVs of the GO-8267 and GO-7503 datasets overlotted, and the field analyzed by GHE01a shown by the large rectangle. The approximate cluster center is shown by the 'X' and the  $24''$  core radius is shown by the large circle. X-ray sources with optical identifications are labeled with small circles for CVs, larger circles for MSPs or qLMXBs and squares for active binaries (in each case the *HST* positions, shifted to the *Chandra* frame, are used to plot the optical IDs). Marginal optical counterparts are not shown. Sources near the cluster center are labeled in Fig. 2. Note the almost complete lack of active binaries discovered in the regions observed only by the GO-7503 program, because of the lack of high quality time series.

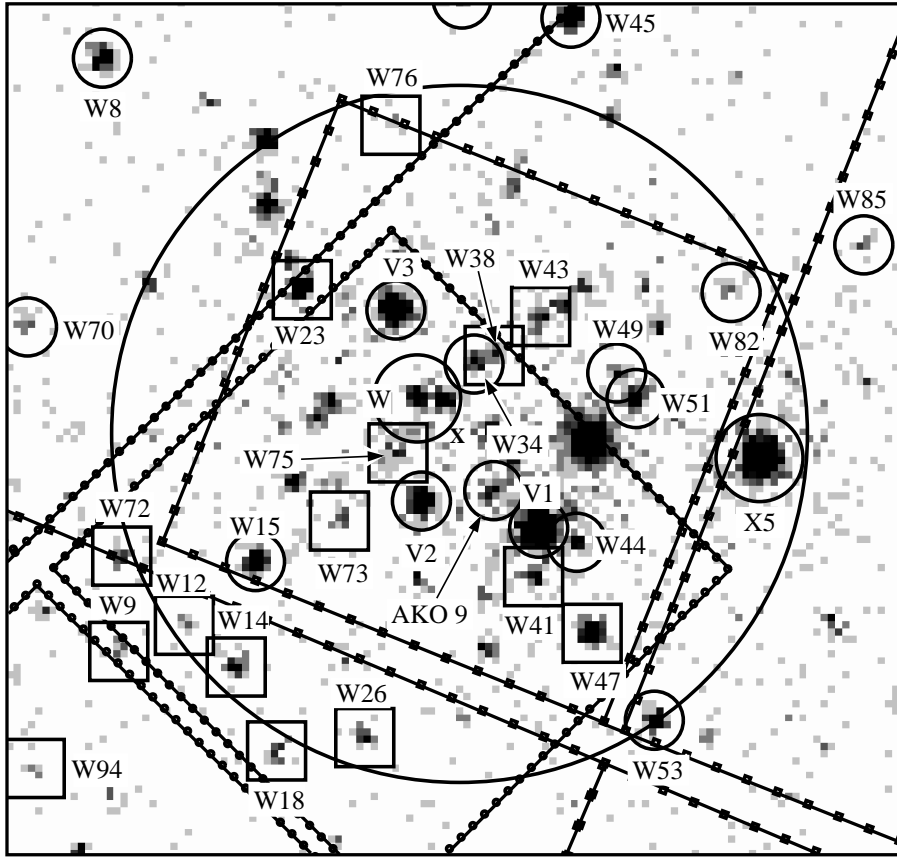


FIG. 2.— A close-up of the central region of Fig. 1, with use of the same labeling. Again, the *HST* positions, globally shifted to the *Chandra* frame, are used for plotting the positions of the optical IDs.

TABLE 1  
*Chandra* SOURCES OUTSIDE GHE01A LIST BUT WITHIN *HST* FoV

<i>Chandra</i> source number (W#)	RA	Dec	medcts <sup>a</sup>	sfcts <sup>b</sup>	hdcts <sup>c</sup>
115	00:24:17.24(2)	-72:04:46.3(1)	3.6	3.8	0.0
120	00:24:11.12(1)	-72:06:20.13(5)	66.2	38.6	33.5
121	00:24:05.16(3)	-72:06:04.3(1)	12.6	8.8	0.0
122	00:24:03.86(1)	-72:06:21.80(7)	46.2	27.7	20.5
137	00:24:18.68(4)	-72:06:02.8(1)	3.8	0.0	0.0
140	00:24:09.22(2)	-72:05:43.7(1)	6.7	4.8	0.0
141	00:24:07.19(3)	-72:04:46.33(8)	5.0	5.2	0.0
142	00:24:04.27(3)	-72:04:20.2(1)	8.3	0.0	0.0
145	00:23:54.60(3)	-72:06:07.7(0)	2.9	0.0	0.0
163	00:24:25.21(4)	-72:05:07.4(1)	6.8	6.8	0.0
167	00:24:10.24(3)	-72:04:01.7(2)	5.7	0.0	0.0
168	00:24:05.96(5)	-72:03:46.5(0)	2.9	0.0	0.0
169	00:24:03.73(0)	-72:05:17.0(0)	1.6	0.0	0.0
182	00:24:19.43(3)	-72:04:31.0(1)	2.7	2.8	0.0
184	00:24:10.52(4)	-72:05:28.8(1)	4.6	0.0	0.0

<sup>a</sup>medcnts = counts in 0.5–4.5 keV band

<sup>b</sup>sfcts = counts in 0.5–1.5 keV band

<sup>c</sup>hdcnts = counts in 1.5–6.0 keV band

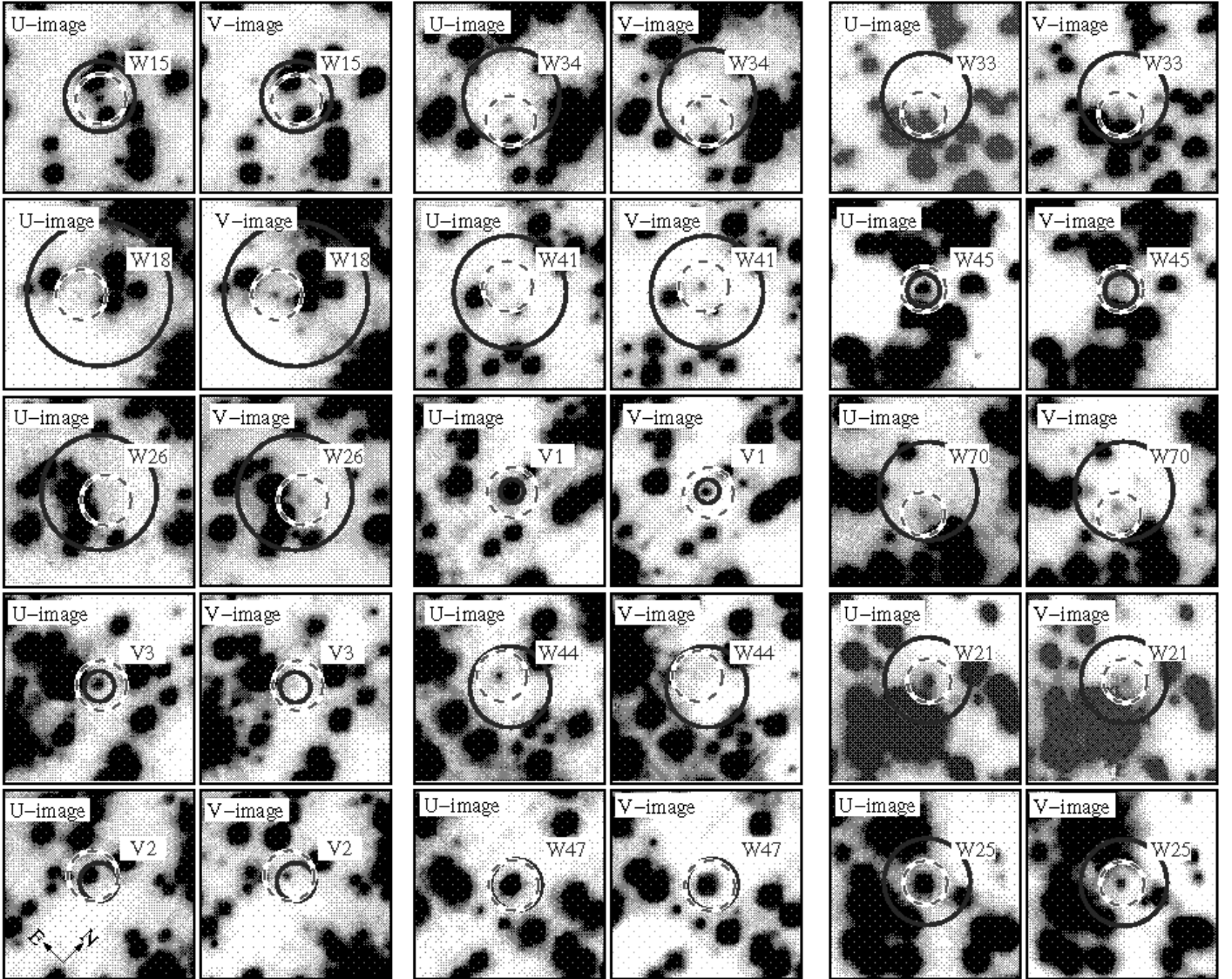


FIG. 3.— A sample of *HST* finding charts for 15 optical identifications from the GO-8267 dataset. Optical IDs for CV candidates in the PC1 chip (W15<sub>opt</sub>, V3, V2, W34<sub>opt</sub>, V1, W44<sub>opt</sub>), the WF2 chip (W33<sub>opt</sub>, W45<sub>opt</sub>, W70<sub>opt</sub>) and the WF4 chip (W21<sub>opt</sub>, W25<sub>opt</sub>) are shown, plus optical IDs for active binary candidates in the PC1 chip (W18<sub>opt</sub>, W26<sub>opt</sub>, W41<sub>opt</sub>, W47<sub>opt</sub>). W34<sub>opt</sub> may also be an MSP. In each case the deep, oversampled images in F336W ('U') and F555W ('V') are shown. The solid circles show the  $4\text{-}\sigma$  errors (the *Chandra* error and the systematic errors for the *Chandra-HST* transformation added in quadrature) and the dashed circles show the candidate optical IDs (radius =  $0''.2$  for the PC1 chip and  $0''.3$  for the WF chips). The CV candidates are all relatively bright in the *U*-band, and the active binary candidates are mostly brighter in the *V*-band.

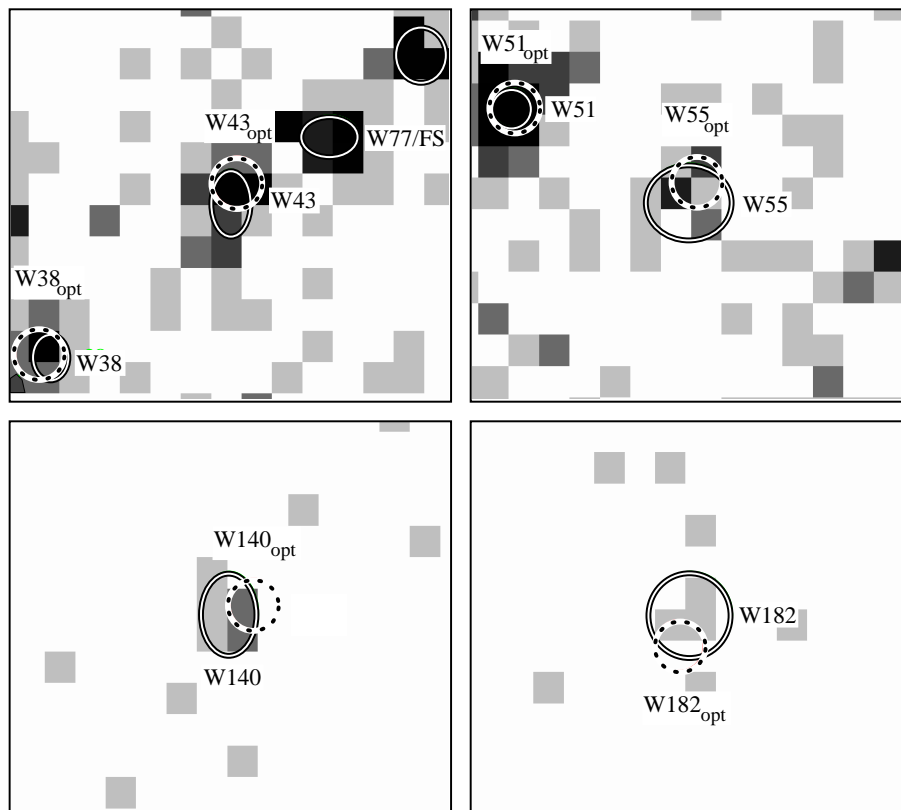


FIG. 4.— *Chandra* images for 4 optical counterparts that are relatively marginal, based on astrometry. The solid lines show the *Chandra*  $5\text{-}\sigma$  error ellipses and the dashed lines show the position of the possible optical counterparts. The ID for W43 is a likely red straggler and therefore is a reasonably secure counterpart (the presence of at least two unresolved X-ray sources appears to have skewed the position of the X-ray source). The source W55 also shows evidence of crowding, but W140 and W182 both appear to be relatively isolated sources.

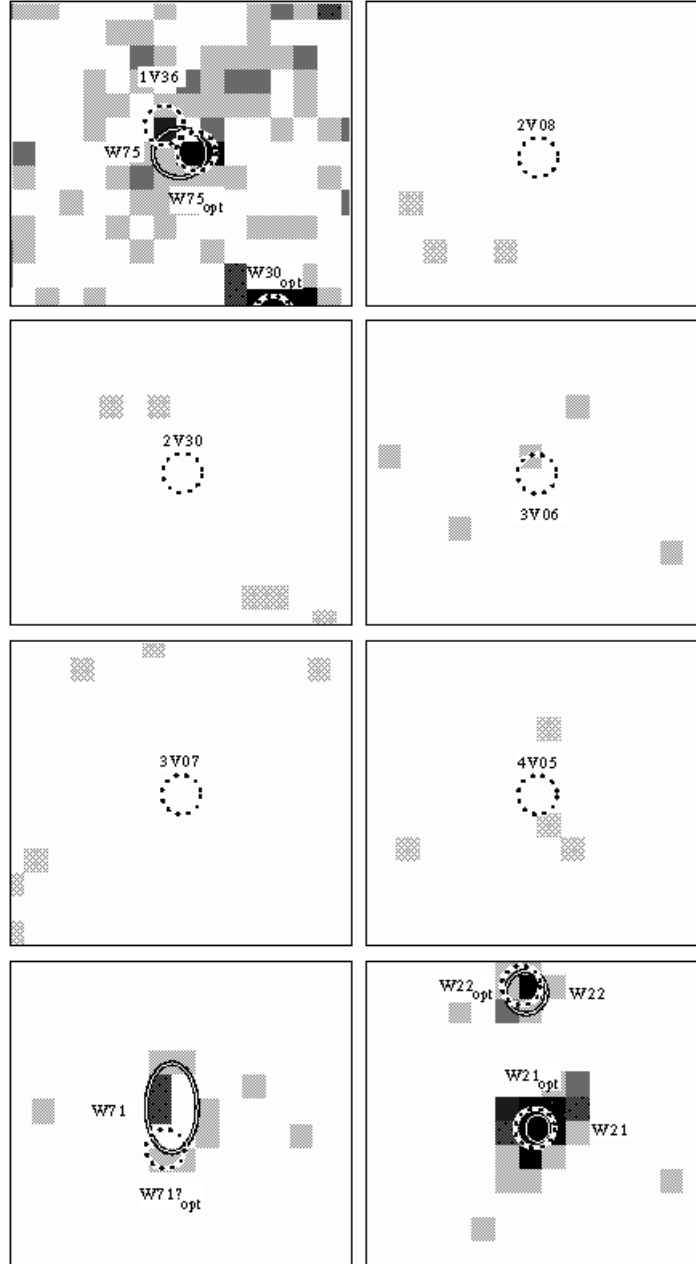


FIG. 5.— *Chandra* image with overlotted circles for the blue variables 1V36, 2V08, 2V30, 3V06, 3V07, 4V05 from AGB01 (the notation [n]V[m] is used where [n] gives the WFPC2 chip number and [m] gives the sequential variable number), plus W71 with its marginal X-ray ID. The same labeling as used in Fig. 4 is adopted. Source W21 is shown because it has optical colors that are very similar to most of the other blue variables. The blue variable 1V36 may correspond to a faint X-ray source, but the other 5 blue variables clearly do not lie near detectable X-ray sources. Error ellipses for the *Chandra* sources found with WAVDETECT are also shown.

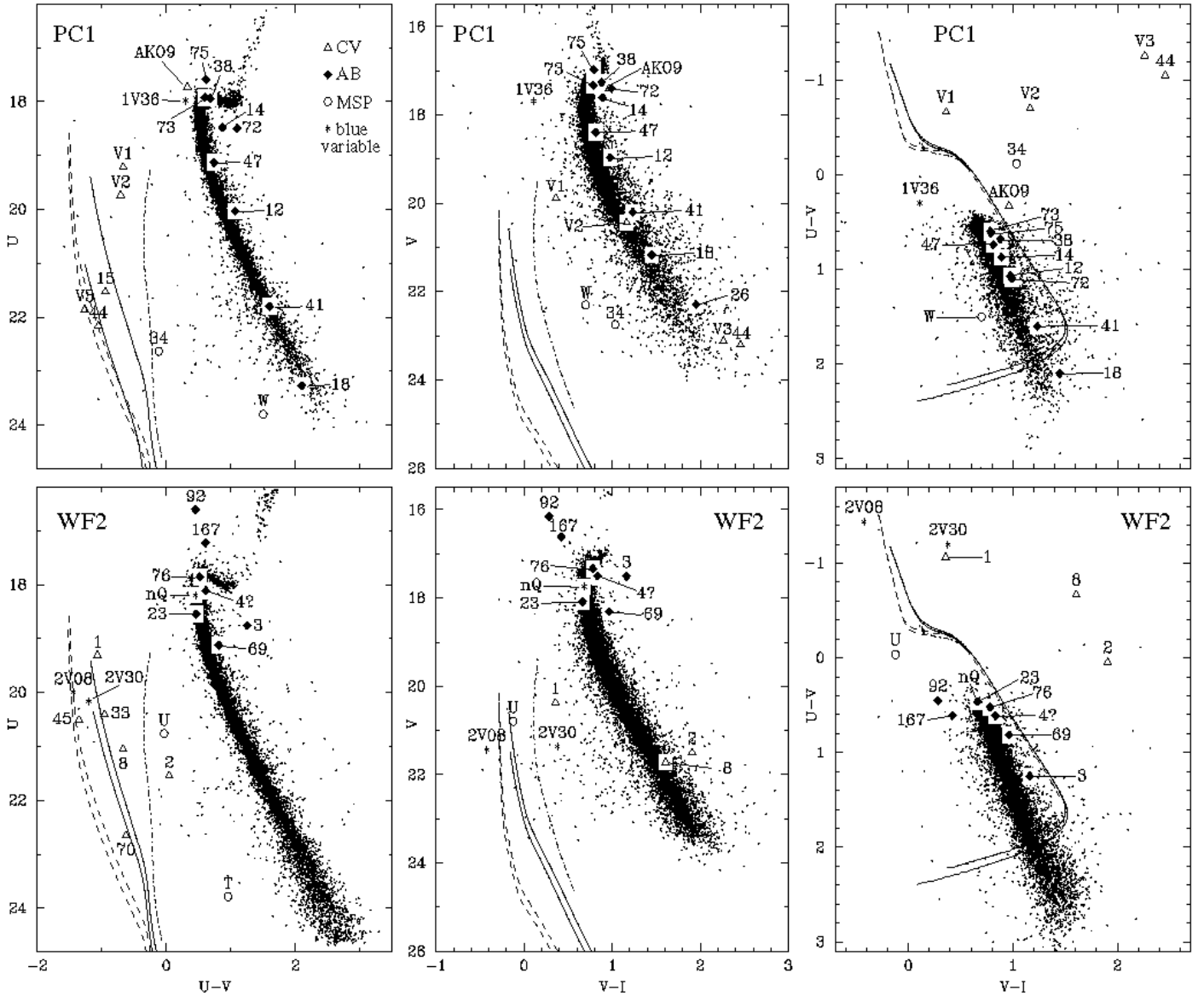


FIG. 6.—  $U$  vs  $U-V$ ,  $V$  vs  $V-I$  and  $U-V$  vs  $V-I$  CMDs for the PC1 and WF2 chips for GO-8267. Optical counterparts for *Chandra* sources are shown with numerals (W#), except for V1 (W42), V2 (W30) and V3 (W27), the optical counterparts to MSPs 47 Tuc U ('U') and 47 Tuc W ('W') and the possible counterpart to 47 Tuc T. The likely variable near MSP 47 Tuc Q is shown as 'nQ', and the blue variables from AGB01 that appear to be X-ray dim (or in the case of 1V36 a possible weak source) are also shown (see Fig. 5). The two dashed lines show  $0.5 M_{\odot}$  and  $0.6 M_{\odot}$  WD cooling tracks from Bergeron, Wesemael, & Beauchamp (1995), the solid lines show He WD cooling tracks from Serenelli et al. (2001) for  $0.196 M_{\odot}$  and  $0.406 M_{\odot}$  models and the dot-dashed line the  $0.169 M_{\odot}$  model.

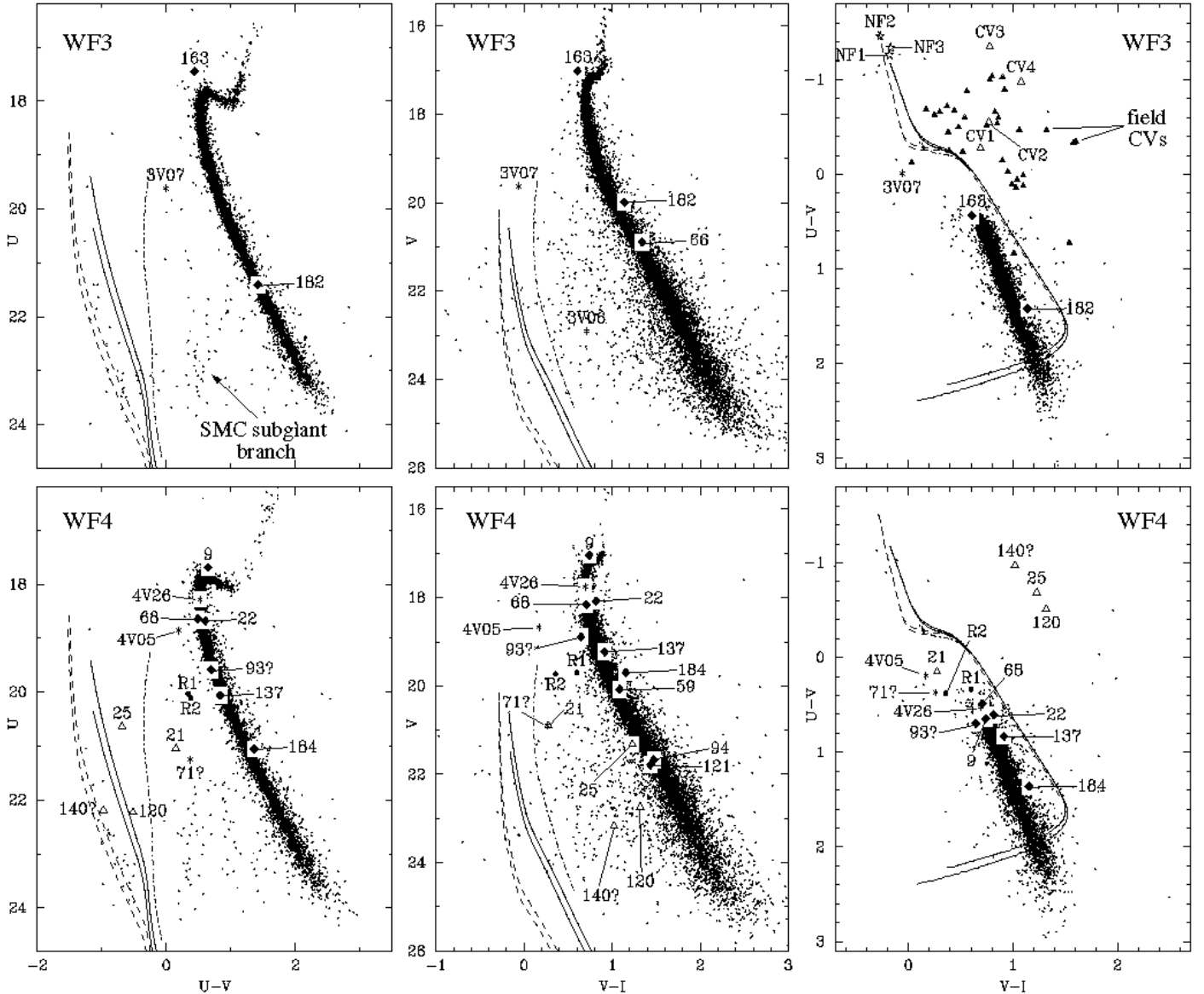


FIG. 7.—  $U$  vs  $U-V$ ,  $V$  vs  $V-I$  and  $U-V$  vs  $V-I$  CMDs for the WF3 and WF4 chips for GO-8267. For WF3 we plot colors for the 4 brightest CVs in NGC 6397 (CV1-CV4) and the 3 brightest He WDs in NGC 6397 (NF1-NF3, where ‘NF’ denotes non-flickerer) from Cool et al. (1998). We also plot (with filled-in triangles) the field CVs with  $UVI$  colors from Zwitter & Munari (1995), Zwitter & Munari (1996), and Munari & Zwitter (1998), plus two RR Lyraes (labeled with filled circles) from the SMC (unpublished work from the authors). Note: (1) the relative lack of CVs falling below the WD cooling tracks in the color-color plot, (2) the populations of cluster WDs detectable in the  $U$  vs  $U-V$  CMDs at  $U-V < 0$  and (3) the subgiant branch of the SMC visible in the  $U$  vs  $U-V$  CMDs (as labeled).

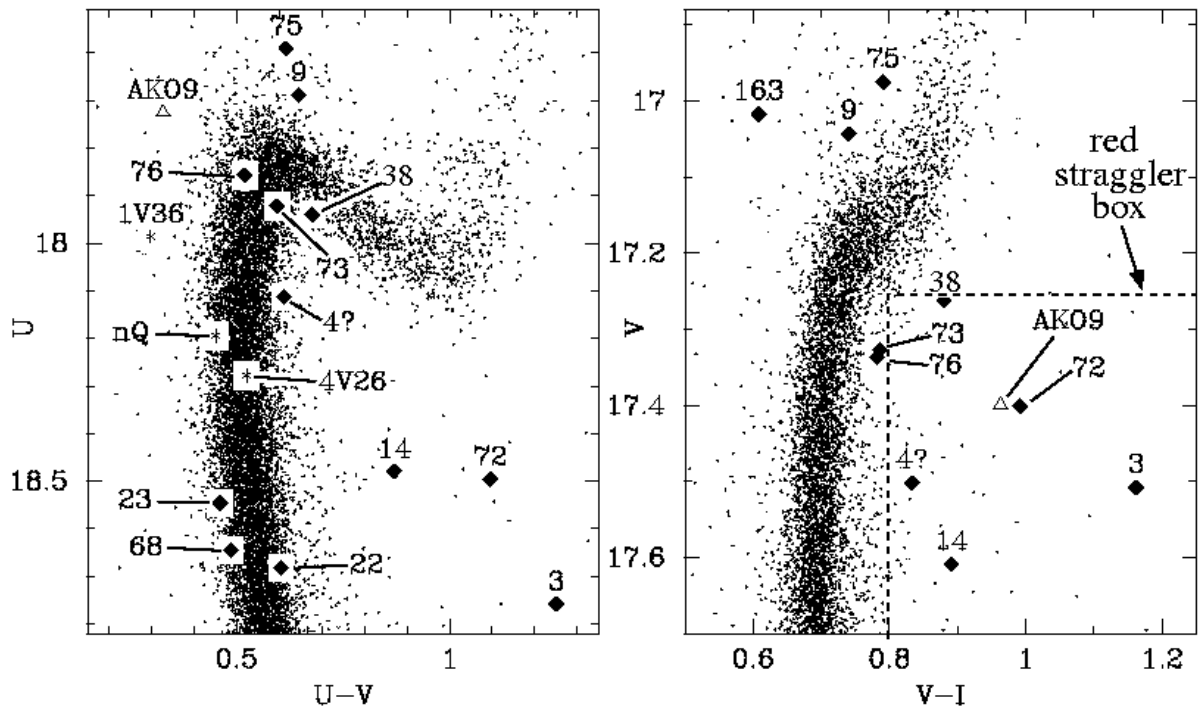


FIG. 8.— A close-up of the region near the MSTO in the  $U$  vs  $U-V$  and  $V$  vs  $V-I$  CMDs for the GO-8267 data. The points for all 4 chips are plotted together, and a portion of the red straggler box from AGB01 is shown ( $0.8 < V-I < 1.5$ ;  $17.25 < V < 17.75$ ). The red stragglers from AGB01 are plotted ( $W3_{\text{opt}}$ , AKO 9, and  $W72_{\text{opt}}$ ) plus other possible red stragglers ( $W4_{\text{opt}}$ ,  $W14_{\text{opt}}$ , and  $W38_{\text{opt}}$ ).

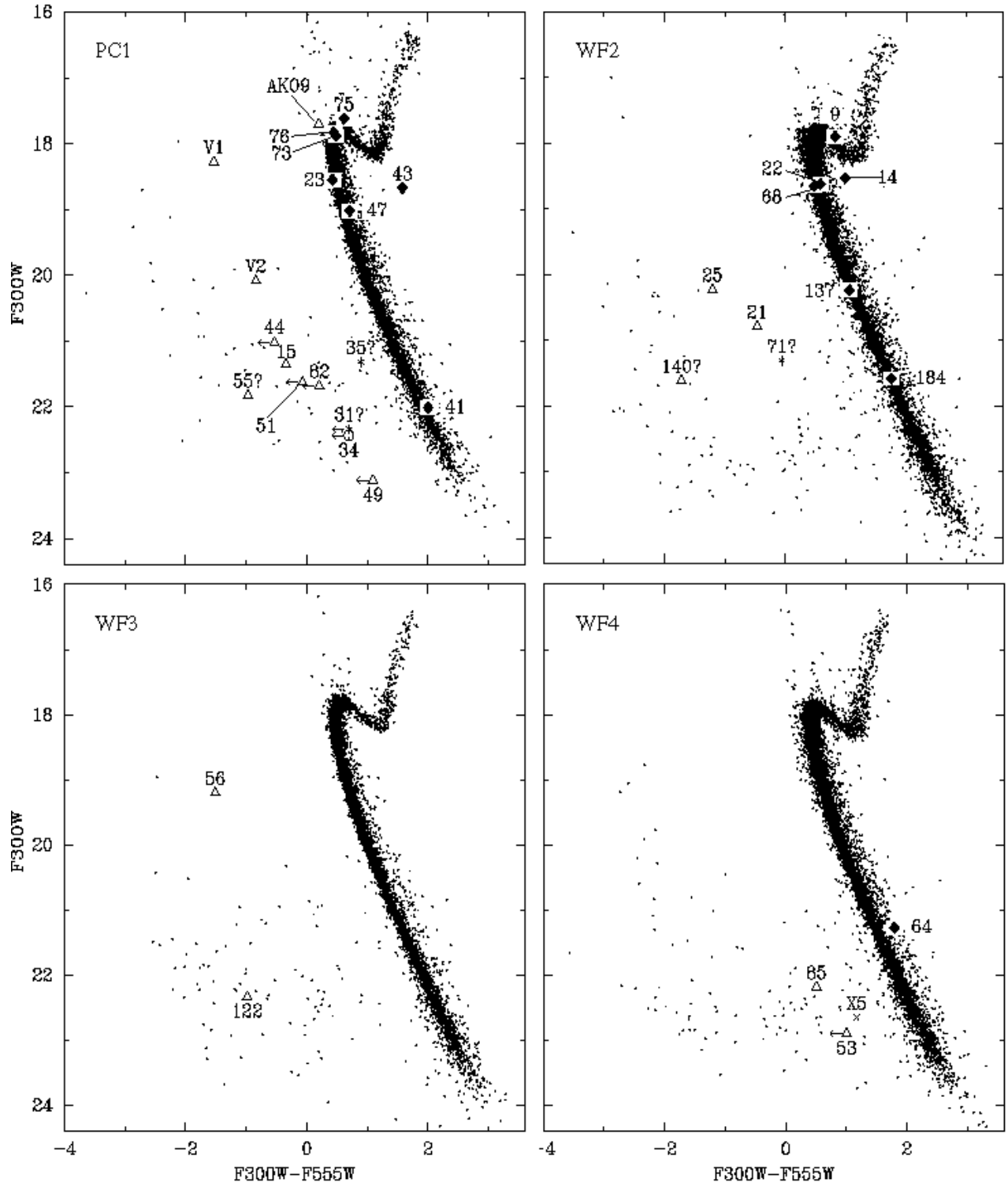


FIG. 9.—  $F_{300W}$  vs  $F_{300W}-F_{555W}$  CMDs for the GO-7503 dataset. Likely or marginal counterparts to X-ray sources are labeled with numerals and symbols (as used in Figures 6 and 7) in the cases where the stars are detected in both  $F_{300W}$  and  $F_{555W}$ . X-ray IDs detected in  $F_{300W}$  but not  $F_{555W}$  are labeled at the red limit with arrows.

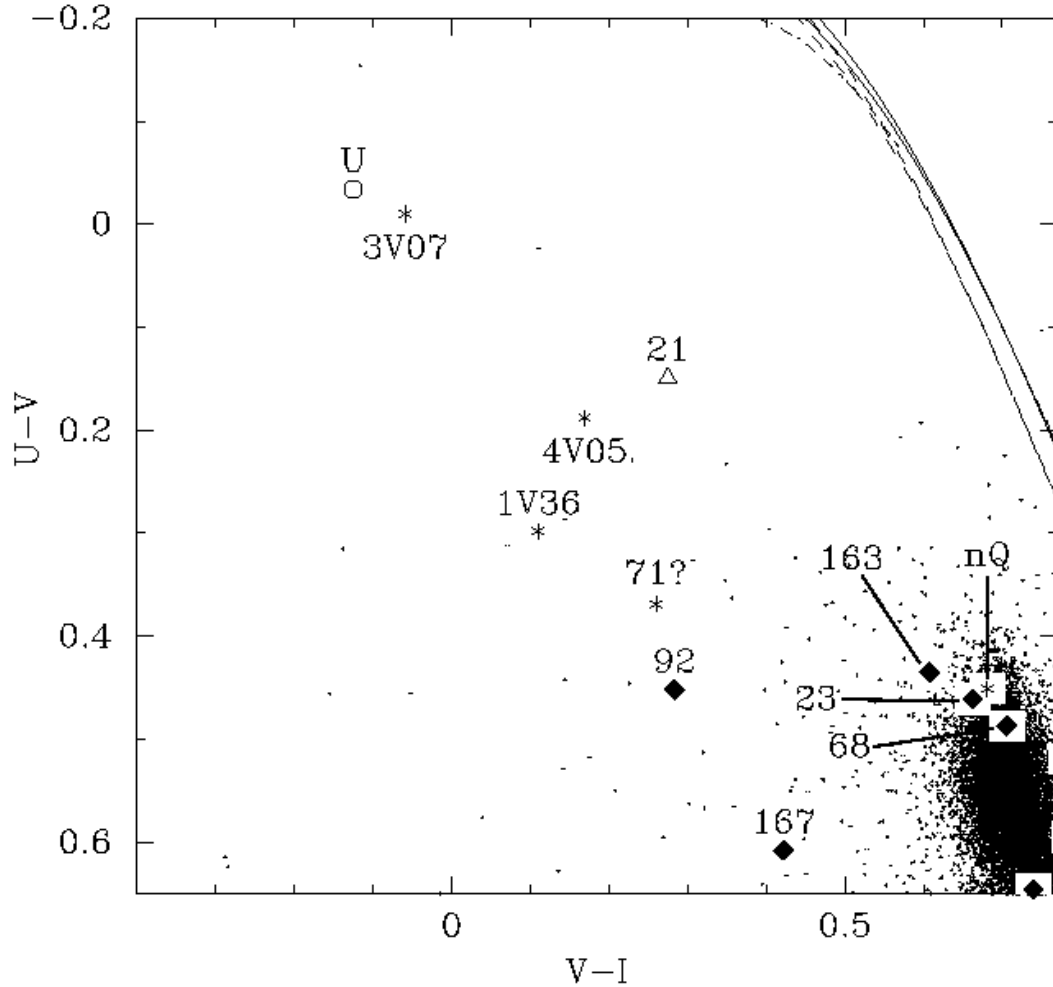


FIG. 10.— A close-up of the  $U-V$  vs  $V-I$  CMD for all 4 WFPC2 chips for GO-8267, showing 4 of the blue variables (1V36, 3V07, 4V05, and the blue variable near W71) that are not obviously associated with WAVEDETECT X-ray sources, plus W21<sub>opt</sub> and the counterpart to 47 Tuc U. The stars W92<sub>opt</sub>, W163<sub>opt</sub> and W167<sub>opt</sub> are blue stragglers.

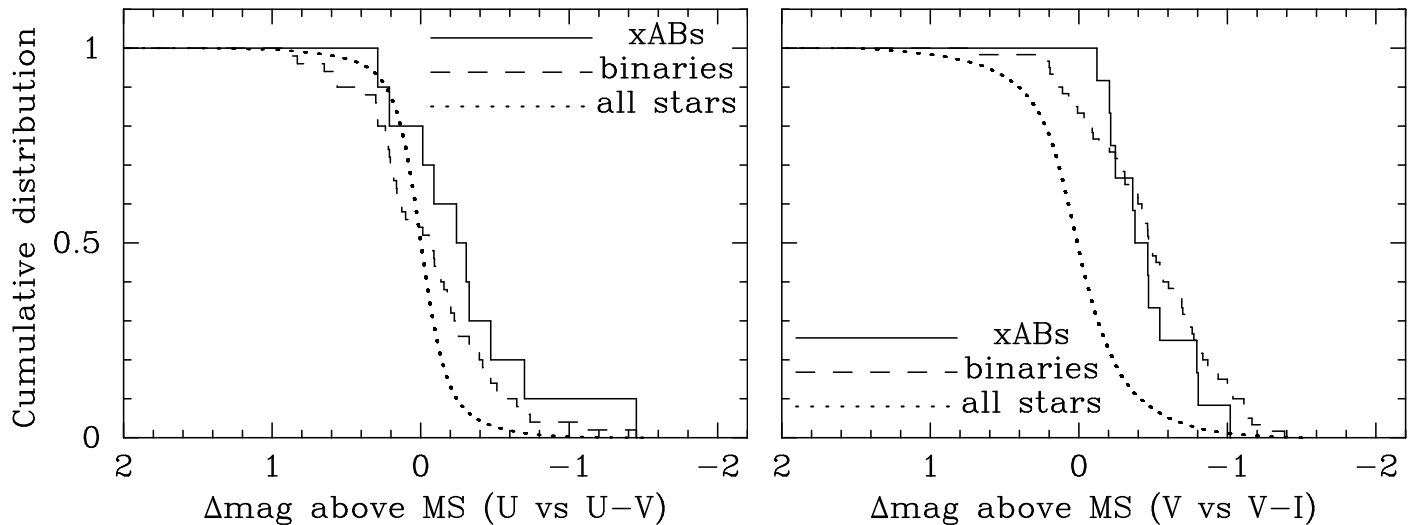


FIG. 11.— Offsets above the main sequence in the  $U$  vs  $U-V$  ( $U > 18.4$ ) and the  $V$  vs  $V-I$  ( $V > 18$ ) CMDs for the AGB01 binaries ('binaries'), the X-ray detected active binaries ('xABs') and the overall population of stars ('all stars').

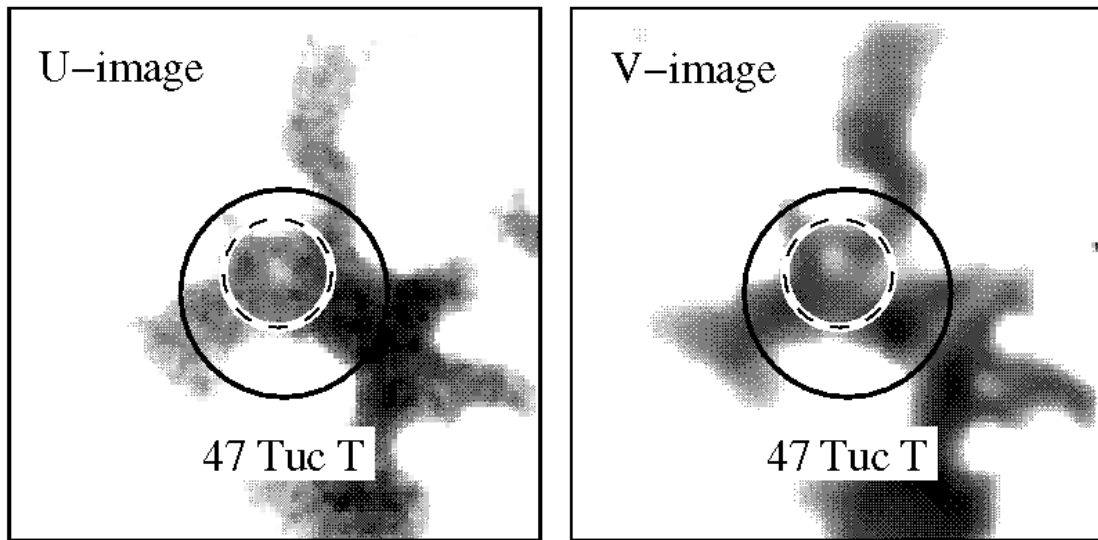


FIG. 12.— Finding charts in  $U$  and  $V$  from the GO-8267 dataset for the possible optical counterpart to the MSP 47 Tuc T. The solid line shows the  $4\sigma$  error circle ( $1\sigma=0''.11$ ) for the MSP and the dotted line shows the faint star detected in the  $U$ -band image. The faint object detected in the  $V$ -band image is clearly a different star because of the significant spatial shift.

TABLE 2  
OPTICAL LOCATION AND OTHER NAMES FOR *Chandra* SOURCES

<i>Chandra</i> W#	GO-8267	GO-7503	AGB01 name	Other names
1	WF2	...	WF2-V09	
2	WF2	...		X13 <sup>c</sup>
3	WF2	...	WF2-V31	
4	WF2	...		
5	WF2	...		
6	WF4	WF2		
7	WF4	WF2		47 Tuc E <sup>j</sup>
8	WF2	...		
9	WF4	WF2	WF4-V06	
10	WF2	...		
11	WF2	...		U <sub>opt</sub> <sup>j</sup> , 47 Tuc U <sup>c</sup>
12	PC1	WF2	PC1-V17	
13	WF2	...		47 Tuc N <sup>j</sup>
14	PC1	...	PC1-V41	
15	PC1	PC1		
16	WF2	...		
17	WF2	...		
18	PC1	WF2	PC1-V29	
19	WF2	PC1		47 Tuc G, <sup>i</sup>
20	PC1	PC1		
21	WF4	WF2		
22	WF4	WF2		
23	WF2	PC1		
24	PC1	PC1		
25	WF4	WF2		X11 <sup>c</sup>
26	PC1	WF2		
27	PC1	PC1		V3 <sup>a</sup> , star #716 <sup>b</sup> , X10 <sup>c</sup>
28	PC1	PC1		
29	PC1	PC1		W29 <sub>opt</sub> <sup>d</sup> , 47 Tuc W <sup>e</sup>
30	PC1	PC1	PC1-V53	V2 <sup>f</sup> , star #5400 <sup>b</sup> , X19 <sup>c</sup>
31	PC1	PC1		
32	PC1	PC1		
33	WF2	...		
34	PC1	PC1		
35	PC1	PC1		
36	PC1	PC1	PC1-V11	AKO 9 <sup>e</sup> , var.#11 <sup>h</sup> , BSS-26 <sup>b</sup>
37	PC1	PC1		
38	PC1	PC1		
39	PC1	PC1		47 Tuc O <sup>j</sup>
40	...	PC1		
41	PC1	PC1	PC1-V19	
42	PC1	PC1	PC1-V47	V1 <sup>i</sup> , UVE-3 <sup>b</sup> , X9 <sup>c</sup>
43	...	PC1		
44	PC1	PC1		
45	WF2	...		
46	PC1	PC1		
47	PC1	PC1	PC1-V08	var. #8 <sup>h</sup>
49	...	PC1		
51	...	PC1		
52	...	WF3		
53	...	WF4		
54	...	PC1		
55	...	PC1		
56	...	WF3		X6 <sup>c</sup>
57	...	PC1		
58	...	WF4		X5 <sub>opt</sub> <sup>k</sup> , X5 <sup>c</sup>
59	WF4	WF3		
60	...	WF4		
61	...	WF4		
62	...	WF4		
64	...	WF4		
65	...	WF4		
66	WF3	WF2	WF3-V08	
67	WF2	...		47 Tuc D <sup>j</sup>
68	WF4	WF2		
69	WF2	...	WF2-V18	
70	WF2	...		
71	WF4	WF2		
72	PC1	...	PC1-V48	
73	PC1	PC1	PC1-V24	
74	WF2	...		47 Tuc H <sup>j</sup>
75	PC1	PC1	PC1-V23	
76	WF2	PC1	WF2-V17	
77	...	PC1		47 Tuc F, <sup>i</sup> S <sup>j</sup>
78	...	WF3		
79	...	PC1		
80	...	PC1		
81	...	WF4		
82	...	PC1		
84	...	WF3		

TABLE 2—*Continued*

<i>Chandra</i> W#	GO-8267	GO-7503	AGB01 name	Other names
85	...	WF4		
86	...	WF4		
87	...	WF4		
90	...	WF3		
91	WF2	...		
92	WF2	...	WF2-V03	
93	WF4	WF2		
94	WF4	WF2		
95	WF2	...		
96	PC1	WF2		
97	PC1	WF2		
98	PC1	PC1		
99	WF4	WF3		
101	...	WF3		
102	...	WF3		
103	...	WF4		
115	WF3	...		
120	WF4	WF2		
121	WF4	WF3		
122	...	WF3		
137	WF4	WF2	WF4-V03	
140	WF4	WF2		
141	PC1	PC1		
142	WF2	...		
145	...	WF3		
163	WF3	...	WF3-V05	
167	WF2	...		
168	WF2	...		
169	...	WF2		
182	WF3	...	WF3-V01	
184	WF4	WF2		

<sup>a</sup>Shara et al. (1996)<sup>b</sup>Ferraro et al. (2001a)<sup>c</sup>Verbunt & Hasinger (1998)<sup>d</sup>Edmonds et al. (2002b)<sup>e</sup>Camilo et al. (2000)<sup>f</sup>Paresce & de Marchi (1994)<sup>g</sup>Auriere et al. (1989)<sup>h</sup>Edmonds et al. (1996)<sup>i</sup>Paresce et al. (1992)<sup>j</sup>Edmonds et al. (2001)<sup>k</sup>Edmonds et al. (2002a)

TABLE 3  
*HST* (GO-8267) DATA FOR COUNTERPARTS TO 47 TUC *Chandra* SOURCES

Source W#	Chip #	$\Delta RA$ ''	$\Delta Dec$ ''	signif.	chance %	$V$	$U - V$	$V - I$	RA <sup>a</sup>	Dec <sup>a</sup>	period (days)	class.
12	1	-0.18	0.11	1.40	0.401	18.96	1.07	0.98	00:24:09.2475	-72:05:04.546	1.128	AB
14	1	0.04	0.08	0.76	0.070	17.61	0.87	0.89	00:24:08.4775	-72:05:07.420	5.02	AB
15	1	-0.01	0.03	0.42	0.405	22.47	-0.94	...	00:24:08.1886	-72:05:00.166	0.17640	CV
18	1	-0.11	-0.10	1.05	0.205	21.17	2.10	1.45	00:24:07.8785	-72:05:13.195	0.528	AB
26	1	-0.00	0.08	0.70	0.058	22.29	...	1.95	00:24:06.5664	-72:05:12.285	0.39386	AB
27	1	0.02	-0.00	0.64	0.018	23.11	-1.26	2.26	00:24:06.0983	-72:04:42.868	0.160	CV
W <sup>d</sup>	1	-0.03	0.06	0.83	0.326	22.30	1.50	0.70	00:24:05.7827	-72:04:48.953	0.13294	MSP
30	1	0.00	-0.07	1.82	0.220	20.44	-0.71	1.16	00:24:05.7208	-72:04:56.015	...	CV
34	1	-0.13	0.13	1.98	2.432	22.75	-0.12	1.03	00:24:04.9369	-72:04:46.589	0.06767	CV/MSP
36	1	0.03	-0.11	1.08	0.879	17.40	0.33	0.96	00:24:04.6452	-72:04:55.300	1.108	CV
38	1	-0.06	-0.05	0.89	0.045	17.25	0.71	0.86	00:24:04.6382	-72:04:46.007	1.866	AB
41	1	0.02	-0.04	0.43	0.020	20.20	1.60	1.23	00:24:04.0533	-72:05:01.221	0.4145	AB
42	1	-0.00	0.01	0.37	0.004	19.88	-0.67	0.36	00:24:03.9773	-72:04:57.885	...	CV
44	1	0.01	-0.11	1.34	0.806	23.20	-1.05	2.46	00:24:03.4124	-72:04:58.856	...	CV
47	1	-0.02	-0.01	0.37	0.003	18.39	0.74	0.81	00:24:03.1840	-72:05:05.123	0.5305	AB
72	1	-0.01	-0.07	0.53	0.043	17.40	1.10	0.99	00:24:10.1782	-72:04:59.780	6.71	AB
73	1	-0.15	0.20	1.89	0.559	17.33	0.59	0.79	00:24:06.9408	-72:04:57.384	2.43	AB
75	1	0.35	-0.03	2.30	1.115	16.98	0.62	0.79	00:24:06.0691	-72:04:52.698	4.36	AB
1	2	-0.01	0.03	0.32	0.019	20.37	-1.07	0.36	00:24:16.7173	-72:04:27.124	0.2405	CV
2	2	-0.02	-0.03	0.45	0.027	21.50	0.04	1.91	00:24:15.6337	-72:04:36.312	0.262 <sup>b</sup>	CV
3	2	-0.10	0.11	1.14	0.035	17.51	1.25	1.16	00:24:14.9180	-72:04:43.454	5.34	AB
8	2	0.00	-0.14	1.31	0.288	21.72	-0.67	1.61	00:24:10.5048	-72:04:25.579	0.11927	CV
U <sup>d</sup>	2	-0.04	0.02	0.26	0.048	20.80	-0.03	-0.12	00:24:09.5995	-72:03:59.607	0.432	MSP
23	2	0.10	0.05	1.29	0.020	18.08	0.46	0.66	00:24:07.5283	-72:04:41.533	0.25744	AB
33	2	0.14	0.19	1.45	0.825	21.40	-0.68	...	00:24:05.1432	-72:04:21.531	...	CV
45	2	-0.02	-0.01	0.27	0.012	21.91	-0.98	...	00:24:03.5197	-72:04:22.856	...	CV
69	2	0.11	0.16	0.84	0.063	18.31	0.81	0.96	00:24:12.3851	-72:04:22.230	3.06	AB
70	2	0.16	0.27	1.86	1.438	23.30	-0.42	...	00:24:11.6261	-72:04:44.077	...	CV
76	2	-0.31	0.10	1.43	0.177	17.34	0.52	0.78	00:24:06.2042	-72:04:30.219	0.633	AB
92	2	-0.04	-0.06	0.29	0.008	16.16	0.45	0.28	00:24:15.4300	-72:04:41.230	1.34	AB
167	2	0.03	-0.20	0.84	0.070	16.62	0.61	0.42	00:24:09.9704	-72:04:01.465	0.37212	AB
66	3	0.06	-0.01	0.34	0.006	20.89	...	1.34	00:24:15.7319	-72:04:51.695	0.2108	AB
163	3	-0.08	0.01	0.38	0.009	17.02	0.40	0.61	00:24:24.9261	-72:05:07.236	0.3450	AB
182	3	-0.19	0.49	2.77	0.369	19.99	1.54	1.14	00:24:19.1672	-72:04:31.339	0.4174	AB
9	4	-0.09	0.08	0.64	0.055	17.04	0.65	0.74	00:24:10.2673	-72:05:06.501	6.13	AB
21	4	-0.03	-0.00	0.22	0.032	20.89	0.15	0.27	00:24:07.4969	-72:05:27.196	0.07223	CV
22	4	-0.11	-0.15	1.09	0.129	18.08	0.61	0.82	00:24:07.5631	-72:05:24.292	2.4494	AB
25	4	0.02	-0.04	0.29	0.014	21.32	-0.68	1.23	00:24:06.8635	-72:05:45.663	...	CV
59	4	0.02	0.01	0.11	0.002	20.08	...	1.08	00:24:00.3385	-72:05:54.156	0.24302	AB
68	4	-0.32	-0.09	1.35	0.412	18.16	0.49	0.71	00:24:13.2434	-72:05:23.372	1.118	AB
94	4	0.05	-0.12	0.61	0.065	21.67	...	1.47	00:24:11.5193	-72:05:14.533	0.27259	AB
120	4	0.19	-0.01	0.94	0.275	22.74	-0.30	1.33	00:24:10.8120	-72:06:19.926	0.220?	CV
121	4	-0.08	0.11	0.62	0.070	21.78	...	1.44	00:24:04.9081	-72:06:04.256	0.15784	AB
137	4	-0.24	0.19	1.02	0.354	19.23	0.83	0.91	00:24:18.4695	-72:06:02.872	0.5875	AB
184	4	-0.27	0.32	1.60	0.677	19.70	1.36	1.16	00:24:10.3112	-72:05:29.076	0.7722	AB
Marginal candidates												
4?	2	0.07	-0.10	1.13	...	17.50	0.61	0.83	00:24:13.2008	-72:04:51.114	...	AB?
T? <sup>d</sup>	2	-0.10	-0.05	0.88	...	>22.83	<0.95	...	00:24:08.3049	-72:04:38.786	...	MSP?
71?	4	-0.14	0.82	3.37	11.034	20.88	0.37	0.26	00:24:10.3766	-72:05:17.225	0.09877	CV?
93?	4	0.53	-0.28	2.61	...	18.89	0.70	0.65	00:24:11.6536	-72:05:07.832	0.2266	AB?
140?	4	0.43	-0.17	2.09	4.125	23.16	-0.65	1.02	00:24:08.8636	-72:05:43.491	...	CV?

<sup>a</sup>Coordinates were calculated using the STSDAS task METRIC and archival image u5jm070cr.

<sup>b</sup>X-ray period.

<sup>c</sup>Significant non-periodic variability seen in  $V$  and  $I$  time series.

<sup>d</sup>MSP from Camilo et al. (2000).

TABLE 4  
*HST* (GO-7503) DATA FOR COUNTERPARTS TO 47 TUC *Chandra* SOURCES

Source W#	GO-8267	Chip #	$\Delta RA$ //	$\Delta Dec$ //	signif.	chance %	$F_{300W}$	$F_{555W}$	RA <sup>a</sup>	Dec <sup>a</sup>	class.	variability btw. epochs?
15	Y	1	-0.06	0.06	0.99	0.405	21.17	21.70	00:24:08.4485	-72:05:00.495	CV	
23	Y	1	0.06	0.10	1.56	0.020	18.57	18.12	00:24:07.7475	-72:04:41.833	AB	
27	Y	1	0.02	0.00	0.44	0.018	20.64	>21.64	00:24:06.3484	-72:04:43.184	CV	
30	Y	1	-0.01	-0.06	1.29	0.220	19.90	20.92	00:24:05.9737	-72:04:56.326	CV	yes
34	Y	1	-0.14	0.13	1.95	2.432	23.14	>21.75	00:24:05.1874	-72:04:46.899	MSP/CV	
36	Y	1	0.03	-0.11	1.07	0.879	17.68	17.50	00:24:04.8959	-72:04:55.599	CV	
41	Y	1	0.01	-0.05	0.43	0.020	22.03	20.01	00:24:04.3050	-72:05:01.513	AB	yes
42	Y	1	-0.00	0.01	0.25	0.004	18.10	19.81	00:24:04.2273	-72:04:58.184	CV	
43		1	0.09	-0.35	2.83	...	18.49	17.10	00:24:04.1995	-72:04:43.607	AB	
44	Y	1	0.00	-0.11	1.34	0.806	20.82	>21.56	00:24:03.6633	-72:04:59.147	CV	yes
47	Y	1	-0.02	-0.01	0.41	0.003	19.04	18.31	00:24:03.4351	-72:05:05.413	AB	
49		1	-0.11	-0.07	1.13	1.044	23.40	>22.02	00:24:03.0707	-72:04:47.501	CV	
51		1	0.04	-0.02	0.48	0.130	22.12	>21.69	00:24:02.7856	-72:04:49.258	CV	yes
73	Y	1	-0.17	0.22	2.04	0.559	17.92	17.40	00:24:07.1965	-72:04:57.699	AB	
75	Y	1	0.34	-0.02	2.20	1.115	17.44	17.01	00:24:06.3214	-72:04:53.012	AB	
76	Y	1	-0.29	0.14	1.46	0.177	17.93	17.38	00:24:06.4159	-72:04:30.517	AB	
82		1	0.10	0.22	1.32	2.286	21.50	>21.47	00:24:01.3734	-72:04:41.964	CV	
9	Y	2	-0.10	0.12	1.04	0.055	17.59	17.07	00:24:10.4786	-72:05:06.823	AB	
14	Y	2	0.08	0.06	0.92	0.070	18.55	17.54	00:24:08.7139	-72:05:07.850	AB	
21	Y	2	-0.04	0.02	0.56	0.032	20.61	21.25	00:24:07.7102	-72:05:27.552	CV	
22	Y	2	-0.12	-0.13	1.51	0.129	18.52	18.04	00:24:07.7772	-72:05:24.632	AB	
25	Y	2	-0.02	-0.04	0.88	0.014	20.04	21.43	00:24:07.0828	-72:05:46.041	CV	
68	Y	2	-0.35	-0.07	1.90	0.412	18.75	18.18	00:24:13.4607	-72:05:23.717	AB	
137	Y	2	-0.34	0.20	1.92	0.354	20.24	19.17	00:24:18.6980	-72:06:03.308	AB	
184	Y	2	-0.29	0.33	1.97	0.677	21.60	19.83	00:24:10.5264	-72:05:29.422	AB	
56		3	-0.03	0.02	1.53	0.026	22.58	23.32	00:24:02.0617	-72:05:42.315	CV	yes
122		3	0.11	-0.09	1.52	0.172	19.02	20.71	00:24:03.7760	-72:06:21.924	CV	yes
53		4	0.02	-0.02	0.32	0.024	22.00	>21.68	00:24:02.4777	-72:05:11.466	CV	yes
58		4	-0.01	0.00	1.10	0.004	23.88	21.90	00:24:00.9036	-72:04:53.415	qLMXB	yes
64		4	0.02	-0.05	1.34	...	22.47	21.48	00:23:57.6207	-72:05:02.146	AB	
85		4	0.03	0.11	0.73	0.203	21.29	19.48	00:23:59.3432	-72:04:38.738	CV	
Marginal candidates												
31?	Y	1	0.15	0.12	1.68	2.114	22.84	>21.64	00:24:05.6108	-72:05:04.609	MSP/CV?	
35?	Y	1	0.00	-0.03	0.23	0.050	21.14	20.43	00:24:04.9965	-72:05:06.456	CV?	
55?		1	0.20	-0.41	2.39	10.824	21.65	22.80	00:24:02.1545	-72:04:50.426	CV?	
71?	Y	2	-0.17	0.84	4.06	11.034	20.93	21.37	00:24:10.5916	-72:05:17.553	CV?	
140?	Y	2	0.40	-0.13	2.66	4.125	21.57	23.33	00:24:09.0801	-72:05:43.873	CV?	

<sup>a</sup>Coordinates were calculated using the STSDAS task METRIC and archival image u5470101r.

Note. — (1) 9 sources were in both the GO-7503 and GO-8267 FoVs, and have plausible IDs listed in Table 3, but were too crowded in the GO-7503 images to be included here. These sources are: W12, W18, W26, W29, W38, W59, W66, W94 and W121.  
(2) W120 was found very near the edge of the WF2 chip and its photometry is not included here.  
(3) 22 sources were found in the GO-7503 FoV, but were outside the GO-8267 FoV and had no plausible optical counterparts. There are 6 PC1 sources (W40, W54, W57, W77, W79, W80), one WF2 source (W169), 7 WF3 sources (W52, W78, W84, W90, W101, W102, W145), and 8 WF4 sources (W60, W61, W62, W65, W81, W86, W87, W103). W77 is the X-ray counterpart to 47 Tuc F and 47 Tuc S.

TABLE 5  
*HST* (GO-8267) DATA FOR BLUE VARIABLES

Name	$V$	$U-V$	$V-I$	RA	Dec	period <sup>a</sup> (days)
1V36	17.69	0.30	0.11	00:24:06.2184	-72:04:52.168	0.7944
2V08	21.43	-1.44	-0.42	00:24:15.1166	-72:03:36.569	0.4011
2V30	21.36	-1.20	0.38	00:24:14.8416	-72:03:44.793	2.35
3V06	22.90	...	0.71	00:24:25.4577	-72:04:38.204	0.2316
3V07	19.63	-0.01	-0.06	00:24:14.2860	-72:04:54.745	0.3163
4V05	18.67	0.19	0.17	00:24:14.6191	-72:05:40.371	0.2588
71?	20.88	0.37	0.26	00:24:10.3766	-72:05:17.225	0.09877

<sup>a</sup>The orbital period assuming that the observed variations are ellipsoidal